Chemical Science

ROYAL SOCIETY OF CHEMISTRY

REVIEW

View Article Online
View Journal | View Issue

Check for updates

Cite this: *Chem. Sci.*, 2022, **13**, 13978

Recent progress on MOF-based optical sensors for VOC sensing

Yuwei Shen, Antoine Tissot * and Christian Serre*

The raising apprehension of volatile organic compound (VOC) exposures urges the exploration of advanced monitoring platforms. Metal–organic frameworks (MOFs) provide many attractive features including tailorable porosity, high surface areas, good chemical/thermal stability, and various host–guest interactions, making them appealing candidates for VOC capture and sensing. To comprehensively exploit the potential of MOFs as sensing materials, great efforts have been dedicated to the shaping and patterning of MOFs for next-level device integration. Among different types of sensors (chemiresistive sensors, gravimetric sensors, optical sensors, *etc.*), MOFs coupled with optical sensors feature distinctive strength. This review summarized the latest advancements in MOF-based optical sensors with a particular focus on VOC sensing. The subject is discussed by different mechanisms: colorimetry, luminescence, and sensors based on optical index modulations. Critical analysis for each system highlighting practical aspects was also deliberated.

Received 3rd August 2022
Accepted 4th October 2022

DOI: 10.1039/d2sc04314a

rsc.li/chemical-science

Open Access Article. Published on 05 lokakuuta 2022. Downloaded on 8.6.2026 20.57.17.
This article is licensed under a Creative Commons Attribution-NonCommercial 3.0 Unported Licence.

1. Introduction

Air pollution has become a growing concern worldwide. Specifically owing to the recent pandemic, the time people spend indoors has escalated, which comes with a higher risk of indoor pollutant exposure. Volatile organic compounds (VOCs) are an entire set of vapour-phase atmospheric organics (excluding CO and CO_2) associated with relatively high volatility, due to their high vapour pressures and low boiling points at ambient temperature and pressure. Common species of VOCs include (apolar) alkanes, alkenes, aromatic hydrocarbons, and heteroatom-containing (polar) organic compounds. VOC exposure can cause acute and long-term health issues depending on exposure durations and doses. A direct example is the sick building syndrome, where people in a building experience acute symptoms such as eye, nose, or throat irritations, headaches, fatigue, *etc.* that disappear after exiting the building. Besides, odours generated by VOCs are capable of inducing psychological negative effects. Long-term chronic exposure to certain VOCs can also cause adverse health impacts including cancers and liver, kidney or central nervous system damage.[1] Compounds of major concern include benzene, toluene, xylenes, styrene, acetaldehyde, formaldehyde and naphthalene, which are classified by the European Commission as the priority pollutants to be regulated. Specifically, benzene, formaldehyde, acetaldehyde, and naphthalene are considered carcinogenic.[2] Given the possible health risk caused by VOC exposures, it is imperative to monitor the ambient concentrations of VOCs.

Identification of individual components of VOCs in air samples can be achieved in laboratories *via* analytical methods using gas chromatography (GC) coupled with flame ionization detection (FID), electron capture detection or mass spectrometry (MS).[3] However, these laboratory-based instruments are typically bulky in size, time and power-consuming, complex to operate and expensive. Many other types of sensors have therefore become commercially available or established in research for VOC detection to address the aforementioned limitations. Specifically, commercially available techniques include photo-ionization detectors (PIDs), electrochemical cells, metal-oxide-based chemiresistive sensors (MOs), *etc.* These sensors are generally miniature in size, sensitive to a range of VOCs and have a short response time. However, the main concern for these sensors is cross-sensitivity to multiple gases/vapours simultaneously leading to a lack of selectivity and the fact that their response can be largely perturbed by the interfering species. More advanced sensing platforms are therefore emerging. One solution for circumventing lack of sensitivity is to adopt multiplexing approaches, for example, sensor arrays, also known as e-noses. They combine multiple sensors with smart pattern recognition software for improved sensitivity and selectivity. In some cases, employing sensor arrays can realize individual discrimination of each component in vapour mixtures.[4] Coupling MO sensors with porous solids (*e.g.* zeolites) can also enhance the sensing performance by employing the intrinsic chemical affinity of the porous solids for better selectivity and/or pre-concentrating the selected VOCs for improved sensitivity.[5]

Institut des Matériaux Poreux de Paris, Ecole Normale Supérieure, ESPCI Paris, CNRS, PSL University, 75005 Paris, France. E-mail: antoine.tissot@ens.psl.eu; christian.serre@ens.psl.eu

© 2022 The Author(s). Published by the Royal Society of Chemistry

Open Access Article. Published on 05 lokakuuta 2022. Downloaded on 8.6.2026 20.57.17.
This article is licensed under a Creative Commons Attribution-NonCommercial 3.0 Unported Licence.

Metal–organic frameworks (MOFs) are an extensive class of crystalline micro- or meso-porous hybrid materials that have been widely developed and investigated over the past 20 years.[6] MOFs are built with metal cation based nodes and organic linkers linked *via* coordination bonds. A great variety of chemical combinations between metal secondary building units (SBUs) and organic linkers give rise to diverse topologies and extended physical and chemical properties. These remarkable properties often include tailorable porosity, high surface area, chemical/thermal stability, *etc.*[7,8] MOFs are therefore of great interest for multiple applications, such as gas separation,[9–12] gas storage,[13,14] catalysis[15–17] and bio-applications,[18–20] among others.

MOFs are also appealing candidates for sensing applications owing to the following reasons: (1) their intrinsic porosity can favour diffusion, absorption, and/or interactions with analyte molecules; (2) they can provide various active sites, for instance open metal coordination sites as well as possible intermolecular coupling between analytes and ligands (hydrogen bonds, π–π interaction, *etc.*). These sites can consequently favour sensitive and selective binding with the target gas molecules; (3) their tunable pore size can enable the molecular sieving phenomenon, which can also improve selectivity; (4) the host–guest interactions can lead to detectable changes in chemo-physical properties (resistance, mass, magnetism, colour, *etc.*), in favour of further signal transduction and quantification; (5) the reversible physisorption process assures the reusability of MOFs; in the case of chemisorption, irreversible responses may appear, yet induce higher sensitivity and selectivity.[21–25] Abundant research has been conducted applying MOFs to the design of various types of gas/vapour sensors, including chemiresistive sensors, capacitive sensors, gravimetric sensors, and optical sensors.[23,26–33] Among these categories, colorimetric and optical sensors are highly attractive due to their apparent advantages such as immunity to electromagnetic interferences, capabilities of remote sensing, facile operations, and direct naked-eye detection.

The sensing process generally involves selective adsorption of targeted molecules. MOFs feature attractive aspects for gas adsorption and capture, especially for VOCs. Functionalization of organic ligands is a powerful approach to not only systematically tailor the pore size and aperture of the MOF structure,[34] but also modify the chemical properties of MOFs including hydrophilicity and hydrophobicity, leading to desired sorption properties. It is also possible to combine multiple species of organic linkers in one framework, namely multivariate (MTV)-MOFs. Such a structure is proven to provide a more complex pore environment and exhibit better sorption and separation performance.[35] Besides, defects in MOFs are a unique element to tune the adsorption properties. Missing nodes and missing linkers are the two defects that are mainly observed. The formation of defects in MOFs can change the pore size, rigidity, flexibility and density of the framework. Specifically, missing linker defects lead to more open metal sites, which can favour sorption processes.[36] However, increasing the number of defects in MOF crystals can possibly compromise their chemical stability.

This review summarizes the recent progress of MOF-based optical sensors, with specific highlights for VOC sensing. We will first outline the state of the art in the patterning techniques of MOFs that facilitate the integration of MOFs into different platforms. The next parts focus on the latest advancements of MOF-based optical sensors, which are categorized by sensing mechanisms: colorimetric sensing, luminescent sensing and sensing based on optical index modulation. In particular, the section on optical-index-based sensors describes the development of MOFs incorporated with Fabry–Perot interferometers, Bragg stacks, diffraction grafting, colloidal film engineering, optical fibres, micro-ring resonators, surface resonance and surface-enhanced Raman scattering. Finally, we conclude by highlighting the opportunities and challenges of MOF-based optical sensors with critical insight for their further practical applications.

2. Patterning techniques of MOF thin films

In order to exploit the great potential of MOFs for sensing applications, it is vital to integrate MOFs onto substrates for further real device construction. To date, diverse techniques have been addressed to fabricate MOF films with various substrates, including *in situ* direct growth from hydro/solvothermal synthesis,[37,38] electrochemical deposition,[39] colloidal deposition *via* spin/dip coating,[40,41] atomic layer deposition[42–44] and layer-by-layer epitaxy.[45–47] Each method has its attributes for producing films with different thicknesses, preferred orientation, morphology and mechanical properties. Numerous reviews have been written on this topic, covering various aspects ranging from general fundamentals to advanced practical implementations of MOF films.[48–58] In the following, we describe the most investigated methods for MOF film preparation.

2.1 *In situ* growth

In situ direct growth is one of the most straightforward methods where the substrate is placed in the reacting solution and film growth happens simultaneously during the synthesis. The choice of substrate is critical for this approach despite its ostensible simplicity. Indeed, the surface structure and chemical composition of the substrate influence the nucleation, anchoring and adhesion processes of the MOF particles. For example, some metal oxide surfaces with basicity can form strong covalent bonds with the complexing groups from acidic linkers (carboxylates, phosphonates…), accordingly anchoring the MOF. On the other hand, naturally acidic surfaces such as silica (SiO_2) do not favour the growth of most carboxylate MOFs.[59] Metal pieces[37,60,61] and polymers[62] have also been employed as substrates for successful MOF film installation. The thickness of these films is typically related to the reaction time and falls within the range of a few micrometers.[48] However, control of polymorphism can be complicated and conditions may vary for different MOFs for *in situ* grown films.[63,64]

Open Access Article. Published on 05 lokakuuta 2022. Downloaded on 8.6.2026 20.57.17.
This article is licensed under a Creative Commons Attribution-NonCommercial 3.0 Unported Licence.

Self-assembled monolayers (SAMs) are active molecules attached to the surface of substrates.[65] Tail functional groups (*e.g.* carboxylic acid) on a SAM can be used to coordinate metal centres or SBUs from the mother solution, therefore promoting the nucleation and growth of MOFs.[66] Deploying SAMs can also lead to patterning MOF films *via* micro-patterning techniques,[67] which will be discussed in the next section. Various MOF films have been developed on SAM functionalized substrates (Au, SiO_2, Si, FTO, *etc.*).[38,59,68–71] Noticeably, exchanging functionality of the SAM layer can consequently in some cases impact the nature of the MOF that is formed[61] and/or tune the orientation of formed crystals.[51,59,72] One major disadvantage of this approach is the compatibility between the high reaction temperature for hydro/solvothermal MOF synthesis and temperature-sensitive substrates. However, some MOF films can be grown at room temperature under certain conditions.[71–73] In addition, the complex preparation process and limited control over morphology and defects of the films can still be problematic.[48]

2.2 Liquid phase epitaxy

Unlike one-pot direct growth of MOF films, liquid phase epitaxy (LPE) alternatively grows MOF films layer by layer through immersing substrates into separated solutions of the metal cation precursor and the ligand in a stepwise manner.[57] Epitaxially grown MOF films are also defined as surface-mounted MOFs (SURMOFs), which consist of highly oriented ultrathin MOF multilayers instead of crystalline grains. SURMOF growth is generally conducted from room temperature to 60 °C in ethanol, which are milder conditions than the usual ones used for *in situ* growth.[45] These films tend to be very smooth with a roughness at the molecular level. The thickness and crystallite domain size can be precisely controlled by considering an ideal layer-by-layer growth mechanism.[48] Despite unlimited choices of organic linkers for SURMOF construction, the metal nodes are to date mainly limited to divalent metals, as mild synthetic conditions are required for SURMOF growth.[74]

SAM substrates are broadly employed in this approach to initiate the nucleation of highly oriented SURMOFs. Similar to *in situ* growth, different functional groups on SAMs also affect the growth orientation of SURMOFs. Likewise, tuning the density of functional groups alters the preferential orientations.[74] Arranging SAM functional groups with certain patterns prior to SURMOF growth can strategically template well-defined, patterned films. Li *et al.* reported ZIF-8 film patterning by arrangement of 1-octadecanethiol(ODT)/16-mercaptohexadecanoic acid (MHA) groups with micro-contact printing on gold substrates.[75] The selective growth of ZIF-8 on the ODT SAM surface leads to a dot patterning of the film. By switching the solvent from water to methanol, ZIF-8 only nucleated on the MHA surface and produced a negative pattern. Several research groups have also demonstrated combining LPE methods with microprint contact techniques,[75] lithography[76] and spray coating[77] to pattern the films.[74]

It is also possible to couple the Langmuir–Blodgett (LB) technique with layer-by-layer deposition for fabricating MOFs with a paddle-wheel unit, where 2D nanosheets are first

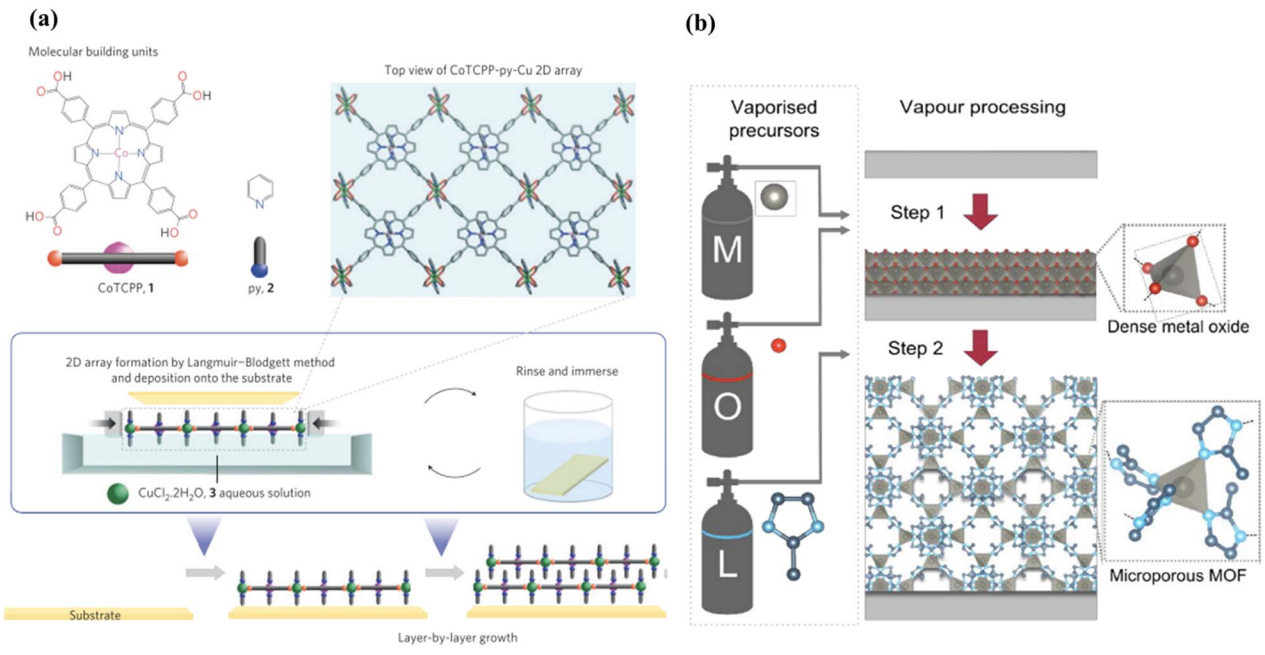

Fig. 1 (a) Schematic illustration of the fabrication of NAFS-1 with bottom-up modular assembly by combining a layer-by-layer growth technique with the Langmuir–Blodgett method. Reproduced from ref. 78. (b) Vapour-phase deposition of ZIF-8 thin films *via* ALD ZnO films. The procedure consists of a metal oxide vapour deposition (step 1) and a consecutive vapour–solid reaction (step 2). Metal, oxygen and ligand sources are labelled as M, O and L, respectively. Metal oxide deposition can be achieved by atomic layer deposition (M, diethylzinc; O, oxygen/water) or by reactive sputtering (M, zinc; O, oxygen plasma). Atom colours: zinc (grey) oxygen (red), nitrogen (light blue) and carbon (dark blue); hydrogen atoms are omitted for clarity. Illustration reproduced from ref. 78.[81]

© 2022 The Author(s). Published by the Royal Society of Chemistry

Open Access Article. Published on 05 lokakuuta 2022. Downloaded on 8.6.2026 20.57.17.
This article is licensed under a Creative Commons Attribution-NonCommercial 3.0 Unported Licence.

synthesized *via* air–liquid interfacial synthesis, followed by introducing pillar linkers for interlayer connection (Fig. 1a).[78] Extensions of this layer-by-layer strategy also include forming films of multivariate MOFs (MTV-MOFs) and MOFs on MOF structures.[79] Another similar approach named substrate-seeded heteroepitaxy uses metal substrates as direct metal sources matching unit-cells for perfect growth. Falcaro *et al.* fabricated a oriented polycrystalline $Cu_2(BDC)_2$ thin film on $Cu(OH)_2$ nanotubes using this strategy.[80] However, it should be noted that only limited MOFs with certain topologies (*e.g.* paddle-wheel structures) can be constructed by the aforementioned approach. The lengthy synthesis and time-consuming step-by-step process should also be considered. In addition, some MOF synthesis requires harsh conditions including acids, heat or specific solvents, which cannot be used for standard LPE or LB procedures.[48,50,74] A simpler LB route starting from pre-synthesized MOF nanoparticles for film deposition will be discussed in the following section dealing with colloidal deposition.

2.3 Atomic/molecular layer deposition

Vapour-based processes avoid the use of solvents, which can intrinsically overcome the limitations of liquid-based strategies such as toxicity, difficulty in scale-up, surface-tension involving issues, *etc*.[82] One of the well-established techniques is atomic layer deposition (ALD). It has been widely investigated and applied to producing inorganic nanomembranes (*e.g.* oxides, nitrides, elementary metals).[83] Combining ALD with molecular layer deposition (MLD), which is often used with organic molecules can lead to the fabrication of crystalline MOF thin films.[42,43,84] A typical ALD/MLD process consists of layer-by-layer deposition of a metal precursor and an organic linker vapour, with purges of inert gases in between depositing the upcoming layer. The construction of the MOF films occurs through a vapour–solid reaction, where the choice of the metal precursor, the linker exposure time, temperature and humidity require precise control.[82,84] Film thickness can be carefully controlled down to the nanoscale. However, the directly deposited film is amorphous in most cases, but it can be crystallized by post-treatments, for instance, annealing under humid conditions,[43] or subsequent exposure to acid.[44,85] This post-crystallization process consequently changes the morphology and roughness of the film, which counteracts the targeted precise thickness control.

To avoid post-deposition treatments, Ameloot *et al.* fabricated a uniform and compact ZIF-8 film through a vapour-phase transformation from ALD ZnO films to ZIF-8, as shown in Fig. 1b.[81] A recent review by Su *et al.*[82] is suggested for further insight regarding this strategy. The solvent-free strategy makes ALD/MLD appealing to the microelectronics industry,[86] as it can lead to a meticulous tuning of thickness and possesses good potential for scale-up. However, this approach is employable almost only for ZIF materials that are easy to produce but possess limited chemical stability. In addition, the large differences in the unit cell parameters between the initial oxide substrates and the MOF might induce the formation of polymorphs and affect the quality of the films. Besides, the necessity of post-synthetic treatments, requirement of high processing temperature and high cost may impede the practical implementation of this method.[87]

2.4 Colloidal deposition

Another easier option for MOF film fabrication is to use colloidal deposition of pre-formed MOF nanoparticles on a substrate. This strategy requires colloidal-stable suspensions of MOF nanocrystals prior to deposition, where MOFs are dispersed in volatile dispersants. Commonly employed techniques include spin coating, dip coating, spray coating and Langmuir Blodgett deposition.[86] The choice of MOF candidates that can be adopted *via* this approach are with less limitations, even including high-valence metal based MOFs such as MIL-101(Cr), MIL-96(Al) and UiO-66.[88–92] The quality of the resulting films highly depends on the homogeneity of the MOF suspension, where the choice of the dispersant and surfactant can be crucial.[89,90] In this strategy, the MOF suspensions are deposited onto flat substrates, after which solvent evaporates leading to uniform and polycrystalline films. In a recent study, Rauf *et al.* reported a homogenous coating of MIL-96(Al) monolayer thin films onto conductive and insulating polymer threads, evidencing the applicability of this approach to a wide choice of substrates.[91] The deposited films possess the hierarchical microporosity from the MOF and additional meso- to macro-porosity from assembled MOF particles.[40] Moreover, the film thickness is often controllable by tuning the particle size of deployed MOFs, the concentration and viscosity of the MOF suspension, as well as deposition parameters (*e.g.* withdraw speed in the case of dip coating).[21]

This approach is easy to operate and cost-efficient. It can be adapted to a broad range of MOFs, as well as combined with other film fabricating processes (*e.g.* CVD).[92] The roughness and orientation of MOF crystals yet remain uncontrolled and depend on the polydispersity and size of the starting nanoparticles. The density of the film also depends on the kinetics of deposition that controls the packing density of the nanoparticles on the substrate. In addition, the adhesion strength between substrates and MOF colloidal films can be weak, leading to insubstantial mechanical strength.[40] A feasible strategy to reinforce the mechanical strength of MOF colloidal films is by incorporating additives, such as inorganic binders or polymers,[93,94] or *via* functionalizing the substrates.[87]

3. MOF-based optical sensors for VOC sensing

Optical sensors are driven by light–matter interaction in the forms of light absorption, emission, reflection, refraction, scattering or transmission. They are usually composed of a light source, a sensing material that can interact with the analytes and a light detector. The spectrum of commonly employed light sources covers from the UV region to the visible region. Depending on specific techniques, detectable parameters include refractive indices, scattering, absorbance and

Open Access Article. Published on 05 lokakuuta 2022. Downloaded on 8.6.2026 20.57.17.
This article is licensed under a Creative Commons Attribution-NonCommercial 3.0 Unported Licence.

Table 1 MOF-based sensing for VOCs categorized by different mechanisms

Sensing mechanism	MOF	Sensing parameters	VOCs	Response time	LoD	Ref.
Colorimetric	$Co_3[Co(CN)_6]_2$	Co^{2+}	Ethanol	1 min	50 to 500 ppm	96
					$\{[Ni(pzt)_2(H_2O)_2](H_2O)(DMF)\}_n$	Ni^{2+}
	Primary amine and methanol	20 min to 50 min	—	97		
	$[Cu(HL)(DMSO)\cdot(MeOH)]_n$	Cu^{2+} and the phosphonate group	DMSO; methanol	39 h	—	98
	Cu^{I}-1-benzimidazolyl-3,5-bis(4-pyridyl)benzene	Ligand-involved charge transfer process	Aliphatic VOCs	20 min to 2.5 h	1 ppm (alcohols); 10 ppm (CH_2Cl_2, $CHCl_3$)	99
	UiO-67-dmbpy	Ligand-involved charge transfer process	Alkylamines	Immediate response	—	100
	UiO-67-bpy-A	Covalent condensation with amino groups	Formaldehyde	3 h	3 ppm	101
	$[Zn_7(bpybc)_3(o\text{-}BDC)_6]\cdot 2NO_3\cdot 6H_2O$	Radical generation of the viologen ligand	Dimethylamine (DMA)	Immediate response	30% DMA aqueous solution	102
			Ethylamine (EA); propylamine (PA)	Immediate response	—	
			Butylamine; benzylamine	~10 s	—	
	$[Cd_2(ipbp)_2(NO_3)_2]\cdot 2DMF$	Synergistic effects of host–guest interactions	Dimethylamine	2 min	400 ppm	103
	TMU-34	Ligand oxidation	Chloroform	10 s	3 ppm	104
	$\{[Zn(3\text{-}DPMNI)_{0.5}(NDC)]\cdot 3DMF\}$	Host–guest electron transfer	*n*-Butylamine	2 s	300 ppm	105
$[Fe^{II}(BPI)(HBPI)(ClO_4)_2] \subseteq$ MFU-4l(Zn)	Spin-crossover complex	Alcohols	—	—	106	
Luminescence	NKU-128	Chromophore grafting	Toluene; THF; DMF; DMSO	24h	—	107
	$[Cu_4I_4(Py_3P)_2]_n$ (Py_3P = tris(2-pyridyl)phosphine)	Guest-lock-induced luminescence	CH_2Cl_2	<1 s	Saturated vapours	108
			Chlorobenzene	455 s		
	NR~*cc*ZIF-8 film (NR = nil red)	Fluorescent dye	Acetone	5 min	60 ppm	109
			Toluene	5 min	95 ppm	
Fabry–Perot interferometers	ZIF-8	Reflectance	Acetone	<2 s	1000 ppm	110
	HKUST-1 ⊃ TiO_2	Reflectance	Acetone	12.2 s	11.27 ppm	111
	Polyhedral ZIF-8	Reflectance	*n*-Heptane	~250 s	500 ppm	112
Bragg stacks	TiO_2/ZIF-8	Reflectance	Ethanol	4.5 s	10% dosage in 0.1 g h^{-1} flow	113
	TiO_2/HKUST-1			7.7 s		
	TiO_2/CAU-1-NH_2			10.1 s		
	TiO_2/CAU-1	Reflectance	Methanol	18 s	—	114
			Heptane	~5 s	—	
Diffraction grafting	Colloidal ZIF-8; ZIF-8/TiO_2	Refractive index; colour luminance	Styrene	—	57 ppm	115
	MIL-100(Cr)	First order diffraction intensity	Toluene	—	200 ppm	116
Optical fibres	ZIF-8/SiO_2 waveguide	Transmission spectra	Ethanol	—	1.6 ppm	117
	ZIF-8/graphene oxide	Transmission spectra	Ethanol	118 ms	5.26 ppm	118
Long-period grafted (LPG) optical fibre	ZIF-8	Transmission spectra	Ethanol	—	9.8 ppm	119

© 2022 The Author(s). Published by the Royal Society of Chemistry

Open Access Article. Published on 05 lokakuuta 2022. Downloaded on 8.6.2026 20.57.17.
This article is licensed under a Creative Commons Attribution-NonCommercial 3.0 Unported Licence.

Table 1 (*Contd.*)

Sensing mechanism	MOF	Sensing parameters	VOCs	Response time	LoD	Ref.
Micro-ring resonators	ZIF-8	Transmission spectra	Methanol	~30 min	58 ppb	29
			Propylene		29 ppb	
			Benzene		35 ppb	
			Toluene		76 ppb	
			Styrene		99 ppb	
Surface plasmon resonance	ZIF-8	Refractive index	Methanol	30 s	2.5 ppm	120
	ZIF-93		*n*-BuOH		73 ppm	
Surface plasmon polariton (SPP) resonance	ZIF-8	Surface plasmon polariton shift	Methanol	—	0.5 ppm in dry N_2; 8 ppm in 40% humidity	121
			Toluene		90–100 ppb	
Surface-enhanced Raman scattering	Ag nanotubes@ZIF-8	SERS spectra	Toluene	80 s	200 ppm	122
	Au@Ag@ZIF-8	SERS spectra	Dimethyl methylphosphonate (DMMP)	30 s	0.2 ppbV	123
	Ag@ZIF-8	SERS spectra	4-Methanylbenzenethiol (4-MBT)	10 s	50 ppb	124
	MIL-100(Fe)	SERS spectra	Toluene	—	0.48 ppb	27

luminescence, which are typically guest molecule dependent.[95] The sensitivity and limit of detection (LoD), therefore, can be interpreted and quantified by the change in the detected parameters induced by analyte exposure. To be specific, the response of colorimetric sensors is defined as changes in color, while luminescent sensing materials are evaluated according to their luminescence intensity or position change upon stimulation. For optical-index-dependent sensors, their sensitivity is defined by the changes in the monitored indices, *e.g.* peak shift in reflectance/transmission spectra. This section will focus on the different platforms that enable MOF-based optical sensing, especially highlighting their application for VOC detection. Table 1 summarizes the recent MOF-based sensors and their performance based on different sensing mechanisms for VOC sensing.

3.1 MOF-based colorimetric sensing

Colorimetry is one of the oldest analytical techniques for its straightforward visualization of results[95] that is broadly applied in current life, *e.g.* pH scales. The phenomenon of chromism originates from interactions between a responsive centre and a triggering analyte. The range involving intermolecular interactions can go from the weakest van der Waals interactions to bond formation and ligand coordination. The main mechanisms of MOF-based chromism sensing include coordination geometry of transition metal triggered colour change, ligand-based charge transfer and functional MOF-composite based sensing (Fig. 2).

3.1.1 Transition metals. MOFs composed of transition metal ions (Fe, Co, Cu, *etc.*) can change colour upon the sorption of guest molecules. In particular, guest molecules interacting with unsaturated metal sites modify the coordination geometry of the metal ions, thus changing their electronic properties, which eventually afford a detectable change in the optical absorption spectrum of the MOF.[24,125] For example, Chen *et al.* reported a reversible structure transformation of a cobalt-based MOF accompanied by colour change upon H_2O or NH_3 sorption in the liquid phase. The presence of H_2O/NH_3 molecules changes the coordination number of Co^{2+} ions from 4 to 6 and consequently the geometry from tetrahedral to octahedral, leading to a colour change from blue to red.[125]

This principle can also be applied for VOC sensing. Dzesse *et al.* have reported preliminary results of solvatochromic behaviour with a transition metal-based MOF by soaking it in different solvents. The MOF, built with Co^{2+} and 3-(4-pyridyl) benzoate, presents solvatochromism upon sorption of various VOCs including polar protic ethanol and methanol, polar aprotic acetone, DMF, DMA, DMSO and nonpolar aprotic dioxane (colours are shown in Fig. 3a).[126] In this case, the solvatochromic response is accompanied by a phase transition. In addition, a Mn-MOF showing solvatochromic behaviour toward ketone molecules was investigated by Li *et al.*, where the introduced ketone molecules distort the parent framework and brought changes in d–d transition into the visible region.[127]

Vapour-phase VOC induced changes in metal centres have also been achieved. Wang and Chen fabricated a film of

Open Access Article. Published on 05 lokakuuta 2022. Downloaded on 8.6.2026 20.57.17.
This article is licensed under a Creative Commons Attribution-NonCommercial 3.0 Unported Licence.

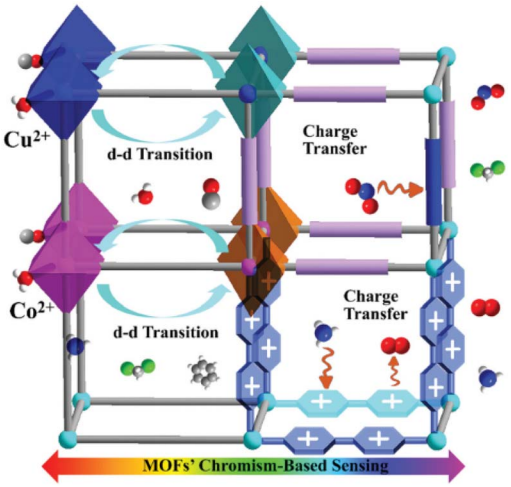

Fig. 2 Illustration of chromism-based sensing mechanisms of MOFs, adapted from ref. 24.

$Co_3[Co(CN)_6]_2$ nanoparticles exhibiting a colorimetric and selective detection of ethanol vapour.[96] The prepared $Co_3[Co(CN)_6]_2$ film undergoes a gradual colour transition from pink to purple when subjected to different concentrations of ethanol vapour (Fig. 3b). Such a colour change was not observed with other solvents (H_2O, methanol, formaldehyde, *etc.*), evidencing the selectivity of the sensor. The detection range of the sensor is from 0.05 mg mL^{-1} to 0.5 mg mL^{-1} of ethanol, with a response time of around 1 min and recovery within a few seconds. The vapochromic behaviour can be explained by the conversion of Co^{2+} ion coordination geometry from octahedral to tetrahedral after ethanol molecules entered the pores and coordinated to Co^{2+} ions. Consequently, the resulting tetrahedral geometry induces a reduction in the d-orbital splitting energy resulting in a redshift in the adsorption spectrum and the colour change of $Co_3[Co(CN)_6]_2$. In another example, Tunsrichon and co-workers introduced a Ni-viologen based 2D MOF $\{[Ni(pzt)_2(H_2O)_2](H_2O)(DMF)\}_n$ (Hpzt = 5-(3-pyridyl)-1,3,4-oxadiazole-2-thiol) with naked-eye chromism in the presence of primary amines and methanol vapours.[97] Upon exposure to NH_3, methylamine, ethylamine and ethylenediamine, the intrinsic blue colour changed by replacing coordinated H_2O molecules with a strong-field amine through forming Ni–N bonds. Bulkier amine vapours did not induce a chromic response due to higher steric hindrance. However, the vapochromism towards amines is irreversible due to the formation of a more stable coordination compound and to the poor chemical stability of these low valence based MOFs. This material also exhibited a selective detection of methanol vapour over other alcohols with a reversible colour change from blue to pale green. The incorporation of MeOH molecules into the MOF distorts the octahedral geometry of Ni^{II} and consequently induces chromism. Vapochromism was also revealed in a single-crystal-to-single-crystal (SC-SC) transformation of a Cu-based MOF.[98] For example, the 3D-MOF $[Cu(HL)(DMSO)\cdot(MeOH)]_n$ (L = triphosphaazatriangulene) exhibits a structural transformation into a 1D-columnar assembly $H_3L\cdot0.5[Cu_2(OH)_4\cdot6H_2O]\cdot4H_2O$ under humid conditions accompanied by a yellow to blue-green colour change of the crystals. A reverse 1D-to-3D transformation structure also occurred upon the sorption of DMSO/MeOH vapours.

Crystals containing Pt(II) complexes can also be coloured due to metal-metal-to-ligand charge-transfer (MMLCT) from the Pt–Pt orbital to the π^* orbital of the organic ligand. Slight modifications of the complex structure upon external stimuli can induce a significant change in the transition energy of MMLCT, resulting in a colour change. For example, Kato *et al.* demonstrated novel Pt(II) diamine based crystals with vapochromic behaviour towards H_2O and alcohol vapours by switching the structures between an amorphous compound and a porous crystalline network.[128,129]

3.1.2 Redox-active ligands. As in the aforementioned (expensive) Pt-based complexes, MOF linkers can also participate as responsive centres towards targeted analytes. Here, the interaction between the guest molecules and the ligands triggers charge transfer processes, accordingly changing the perceived colour of MOFs. For example, a porous Cu^I-MOF reported by Yu *et al.* shows naked-eye chromic detection of polar aliphatic VOCs.[99] The response time of the MOF upon exposure to saturated VOC vapours at ambient temperature ranges from 20 min to 2.5 h. The colorimetric detection limit for alcohols and ketones is about 5 ppm. Single crystal X-ray diffraction analysis evidenced that the guest species are located inside the pores in hydrogen-bonding interactions with the ligand instead of being coordinated to the Cu ions. The UV-visible diffuse reflectance spectra of the VOC-enclosed MOF displayed a gradually broadened absorption band in the visible region. The colour change can be attributed to an intermolecular electron-transfer transition between the ligand and the encapsulated guests. A follow-up study showed that this Cu^I-MOF can be a highly selective visual sensor for recognizing C_2H_2, which was also associated with an intermolecular electron-transfer between the linker and the encapsulated guests.[130]

MOFs composed of redox-active ligands such as viologens,[100–103,131–133] tetrazine derivatives[104] and naphthalene diimide[105] have shown great potential in colorimetric sensing through charge transfer processes. Viologens are 4,4′-bipyridinium derivatives with a particularly electron-deficient nature. Upon interaction with electron-rich molecules, *e.g.* NH_3 and amines, viologen ligands received electrons from the donors and produced radicals, leading to colour changes.[24,134,135] For example, Gao *et al.* synthesized a naphthalene-diimide-based Zn MOF exhibiting photochromic behavior in the presence of various amine vapors (Fig. 4a and b).[105] The nature of its photochromism is from photo-induced electron transfer between the electron-rich guest molecules and electron-deficient MOF. It showed varied colors and response times towards different amine vapors. Specifically for *n*-butylamine (*n*-BUA), the MOF changed its color from yellow to red in 2 s. The similar color induced by *n*-BUA and hydrazine (AH) can be further discriminated by their UV-vis absorption spectra. Yang *et al.* modified the 2,2′-bipyridyl-5,5′-dicarboxylate ligand (bpydc) of the large pore Zr-MOF UiO-67-bpy into *N*,*N*′-dimethyl-2,2′-bipyridinium (dmbpy) through post synthetic *N*-

© 2022 The Author(s). Published by the Royal Society of Chemistry

Open Access Article. Published on 05 lokakuuta 2022. Downloaded on 8.6.2026 20.57.17.
This article is licensed under a Creative Commons Attribution-NonCommercial 3.0 Unported Licence.

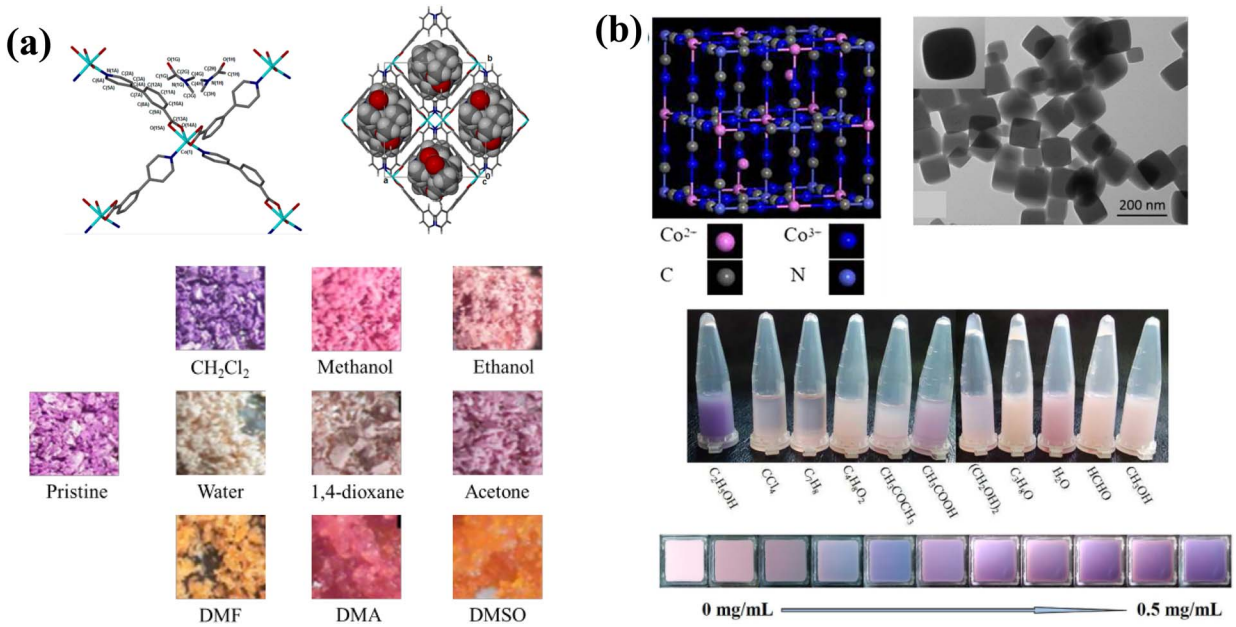

Fig. 3 (a) Coordination environment of Co(II), packing of $\{[Co(3,4pba)_2\text{-}(H_2O)]\cdot 1/2DMF\cdot H_2O\}_n$; and pictures of powdered samples after exposure to different solvents. Figures adapted from ref. 126. (b) Structure of $Co_3[Co(CN)_6]_2$ and TEM image of the nanoparticles; the colour of $Co_3[Co(CN)_6]_2$ films changes from pink to purple gradually with an increasing ethanol concentration gradient. Adapted with permission from ref. 96.

methylation (Fig. 4c).[100] Such modification provides charge-transfer interacting sites for selectively capturing and sensing alkylamines. In this example, the CT interaction between the electron-deficient 2,2′-bipyridinium site and the electron-rich analytes is the driving force for selective molecular recognition and adsorption, as it induces a reversible vapochromism and luminescence quenching. A follow-up study on the same Zr-bpy MOF with *N*-amination modification showed similar chromism behaviour in the presence of amines.[101] Owing to imine condensation, the *N*-aminated MOF also shows a unique colorimetric response to formaldehyde. Another chromic Zn-MOF constructed from a tris-pyridinium ligand was reported by the same group in 2020.[131] The material showed direct colour change towards primary amines (methylamine, ethylamine, *etc.*) and can also be responsive to methanol and ethanol. The mechanism is proposed to be radical formation through spontaneous/photo-induced guest-to-host electron transfer. In addition, the small and interconnected voids due to the 2- fold interpenetration of the MOF give rise to a size and shape selectivity of the chromic process.

Interpenetrated structures of metal-viologen frameworks can stabilize the reduced radicals of viologen ligands and also create multi-bridges for electron transfers, which eventually brings stable and fast responses to multiple stimuli.[102,136] For example, a 7-fold interpenetrated Anderson-like cluster-based Zn(II) MOF $[Zn_7(bpybc)_3(o\text{-}BDC)_6]\cdot 2NO_3\cdot 6H_2O$, reported by Li *et al.*, exhibited visible responses to different types of stimuli including soft X-ray, UV-light, heat, electricity and in the

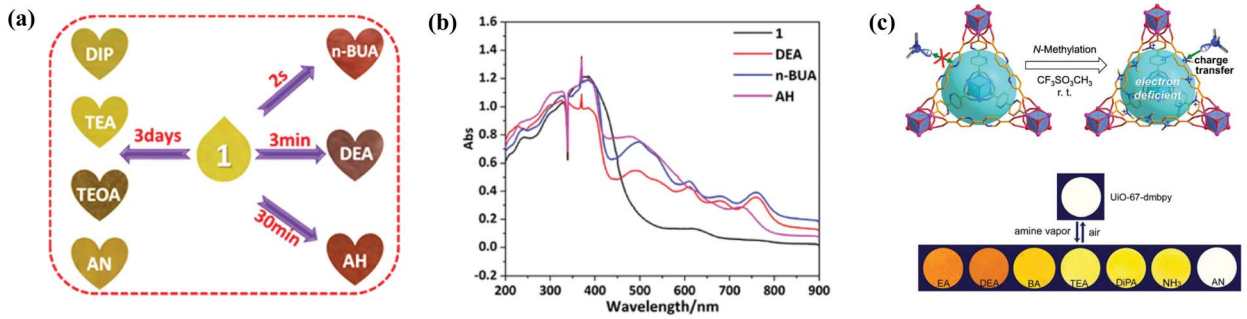

Fig. 4 (a) Color change and response time of $[Zn(3\text{-}DPMNI)_{0.5}(NDC)]$ (denoted as 1 in the figure and following text), (H_2NDC = 2,6-naphthalenedicarboxylic acid and 3-DPMNI = *N*,*N*′-bis(3-pyridylmethyl)-1,4,5,8-naphthalene diimide) in the presence of different amine vapors. (b) UV-vis absorption spectra of 1 in the presence of different organic amines. Figures adapted from ref. 105. (c) Structure of *N*-methylated UiO-67-bpy and its reversible colour change when deposited UiO-67-dmbpy was exposed to amine vapours. *n*-BUA(in a)/BA(in c) = butylamine, DEA = diethylamine, AH = hydrazine, DIP(in a)/DiPA(in c) = diisopropylamine, TEA = triethylamine, TEOA = triethanolamine, AN = aniline, and EA = ethylamine. Figures adapted from ref. 100.

Open Access Article. Published on 05 lokakuuta 2022. Downloaded on 8.6.2026 20.57.17.
This article is licensed under a Creative Commons Attribution-NonCommercial 3.0 Unported Licence.

presence of some organic amines.[102] When exposed to vapours of dimethylamine (DMA), ethylamine (EA), and propylamine (PA), an immediate colour change from the original yellow was observed (pale blue for DEA and purple for EA and PA). Bulkier amines such as butylamine and benzylamine had a prolonged response time of *ca.* 10 s and in these cases, the colour became brown and green, respectively. Solid-state UV-vis and EPR spectra confirmed the generation of viologen radicals after exposure to amines. Such vapochromism was also observed in MOF-PMMA polymer films and is reversible by introducing HCl vapour onto the amine-exposed samples.

Tetrazine derivatives are another type of ligand that can undergo reversible colorimetric responses through redox reactions. Razavi and co-workers developed a dihydrotetrazine-functionalized pillared MOF $[Zn(OBA)(H_2DPT)_{0.5}]\cdot DMF$ (TMU-34) for selective and colorimetric detection of chloroform ($CHCl_3$), where H_2DPT is 3,6-di(pyridin-4-yl)-1,4-dihydro-1,2,4,5-tetrazine is the pillar spacer and H_2OBA is 4,4′-oxybis(benzoic acid).[104] In the presence of $CHCl_3$, a colour change from yellow to pink was observed by the naked eye within 10 s, at the lowest concentration of 2.5×10^{-5} M in both liquid and vapour phases and was regenerated by washing the compound in DMF. In the compound, $CHCl_3$ oxidizes dihydrotetrazine (H_2DPT) into tetrazine (DPT), therefore inducing changes in the geometry and functionality of the pillar spacer, leading to a colour change.

3.1.3 MOF composites. Given the fact that most MOFs are colourless or do not change significantly in colour upon sorption of guests, a rational strategy is to load functional (optically active) guests within the host MOF to achieve visual detection of analytes. Common functional guests include organic dyes (rhodamine, spiropyrans, *etc.*)[137–139] and metal nanoclusters.[140–142] These compounds are either grafted on the metal oxoclusters of MOFs, or loaded into their pores through direct adsorption or covalent grafting[134,143] For example, Koning and co-workers anchored two carboxylate groups of DTNB (5,5′-di-thio-bis-2-nitrobenzoic acid), a bidentate reactive dye, on the unsaturated inorganic node of the mesoporous Zr tetracarboxylate NU-1000 for degradation and visual detection of the nerve agent VX.[143] The octahedral Zr_6 oxoclusters catalyze the hydrolysis of VX and DTNB reacts with the thiol group from degraded products providing a bright yellow colour (Fig. 5a). This dual-functional composite also brings higher detection efficiency compared to the separated DTNB/NU-1000 system. A follow-up study reported the grafting of DTNB onto the large pore Zr trimesate MOF-808 immobilized on cotton forming a MOF/fabric composite enabling practical application of VX degradation and detection.[144] The cloth is capable of visualizing amounts of VX down to 0.16 μg cm^{-2}, which was more sensitive compared to DTNB@NU-1000 (0.8 μg cm^{-2}). It also displayed an improvement in catalytic performance with rapid conversion within 5 min (Fig. 5a and b). However, most MOF composites involve photochromic or luminescent compounds, which require extra light sources to be applied in naked-eye detection. Limited research reported guest chromophore induced colorimetric

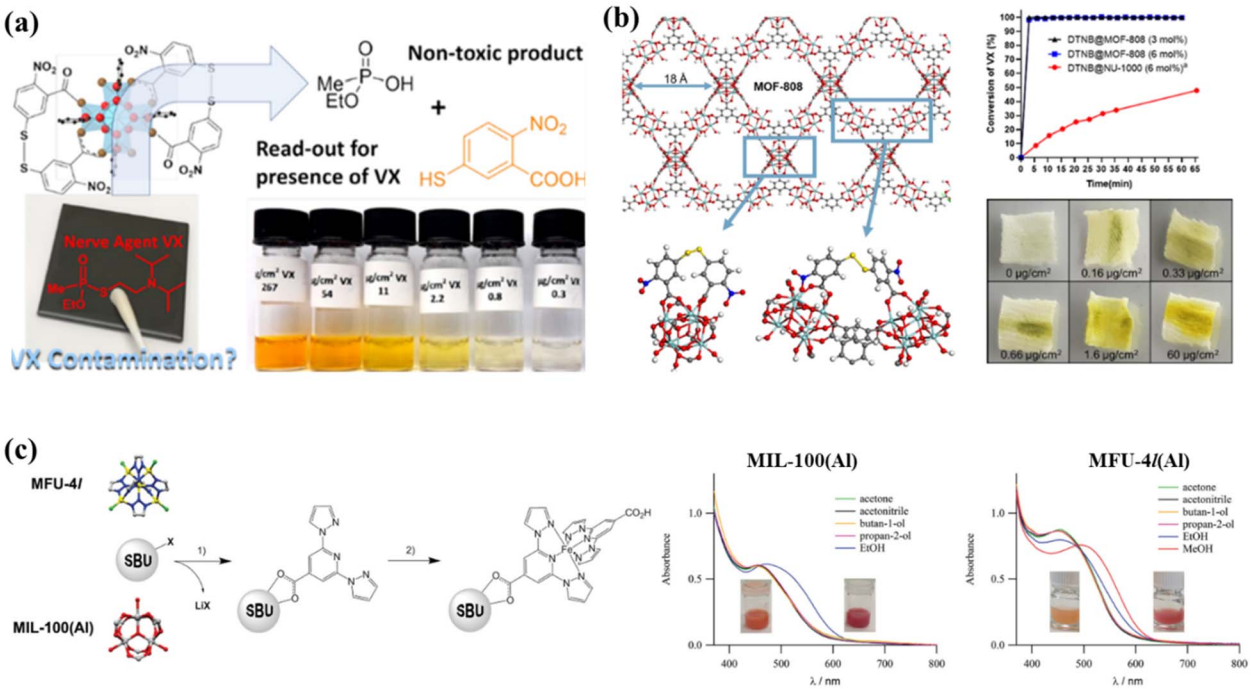

Fig. 5 (a) Illustration of DTNB@NU-1000 for degradation and visual detection of the nerve agent VX.[143] (b) Two anchoring modes of DTNB in MOF-808 and the proposed mechanism of the colour change of DTNB@MOF-808 upon VX degradation. DTNB@MOF-808 degradation kinetics of VX compared to DTNB@NU-1000 degradation kinetics. Photographs of the MOF-textile composite upon contact with VX.[144] (c) Sequential installation strategy for anchoring a SCO complex in a MOF and UV-vis spectra at room temperature of the MOF-SCO composites dispersed in acetone (orange) and EtOH (red) for MIL-100, and dispersed in acetone (orange) and MeOH (red) for MFU-4l.[106]

© 2022 The Author(s). Published by the Royal Society of Chemistry

Open Access Article. Published on 05 lokakuuta 2022. Downloaded on 8.6.2026 20.57.17.
This article is licensed under a Creative Commons Attribution-NonCommercial 3.0 Unported Licence.

sensing, and the majority focused on liquid phase detection of heavy metal ions and organic pollutants.[141,145,146]

Another strategy to achieve colorimetric sensing towards VOCs is through encapsulation of spin-crossover (SCO) complexes into colourless large pore MOFs. As mentioned previously in Section 2, spin-crossover complexes are responsive to external stimuli that are accompanied by a colour change. For example, an Fe(II) complex, $[Fe(HB(pz)_3)_2]$ was confined in diamagnetic and optically-transparent NH_2-MIL-100(Al) and showed a colour change induced by solvent adsorption.[147] Despite that a range of polar to non-polar solvents can induce spin switching accompanied by off-white to red colour change, it is a proof-of-concept that SCO-MOF composites have great potential for sensing applications. Some of us have successfully introduced an Fe(III) SCO compound, $Fe(sal_2trien)NO_3$, into MIL-100(Al) through an *in situ* synthesis.[148] A spin state switching from the inserted $Fe^{III}(sal_2trien)$ cation was observed upon water sorption. Another SCO-MOF system designed by our group was built with $[Fe^{II}(BPI)(HBPI)(ClO_4)_2]^-$ anions anchored in MIL-100(Al) and MFU-4l(Zn), which displayed a selective solvatochromism towards alcohols.[106] In this work, the Fe^{II} SCO complex was anchored on the SBUs of the MOFs *via* the sequential installation strategy. The coordination environment surrounding Fe(II) can be modulated upon alcohol sorption, which leads to a reversible colour change from orange to red (Fig. 5c). This strategy is currently at the very early stage of research but presents great potential for VOC sensing.

3.2 MOF-based luminescent sensing

Luminescent metal–organic frameworks (LMOFs) have been actively explored and investigated for their potential in biological and chemical sensing applications. We will focus in this part on their application towards VOC sensing.

3.2.1 Origins of luminescence in LMOFs. The luminescence in LMOFs commonly originates from the following sources: (1) photo-responsive metal SBUs (*e.g.* lanthanide metal ions and d^{10} transition metal ions), especially trivalent lanthanide ions display sharp emission spectra with wide emission wavelengths from ultraviolet (UV) to near-infrared (NIR) ranges; (2) ligand-centred emission, where the featured ligand typically has extended π-conjugation. Briefly speaking, upon photoexcitation, fluorescence occurs from the emission of a photon from the lowest singlet state (S_1) to the ground state (S_0), showing a typical lifetime in the nanosecond range. With a suitable triplet state (T_1), an intersystem crossing can take place to populate the T_1 state. Subsequently, phosphorescence with a longer lifetime (microsecond to second range) can occur from the photon emission to the ground state (see Fig. 6b). (3) Charge-transfer (CT) based luminescence, which corresponds to the transition from the charge-transfer excited state to the ground state, includes metal-to-metal charge transfer (MMCT), ligand-to-ligand charge transfer (LLCT), metal-to-ligand charge transfer (MLCT) and ligand-to-metal charge transfer (LMCT). (4) Guest-induced emission, by encapsulating luminescent guests such as lanthanide ions, quantum dots, organic dyes, *etc.* in the pores of MOFs. Several books and reviews have described the origin of luminescence in a detailed way, providing a more comprehensive understanding and interpretation of luminescence in MOFs. For example, Cui *et al.* described thoroughly the design and construction strategies for luminescent MOFs categorized by the three elementary units: SBUs, linkers, and guests.[149] Recently, Wang *et al.* carefully depicted the energy transfer mechanisms in LMOFs with a main focus on the most recent research development of LMOFs.[150] Gutierrez *et al.* focused on the confinement of luminescent guests in MOFs, where they gave a comprehensive overview of synthetic methodologies, a systematic discussion of characterization methods, followed by a brief tutorial on the host–guest phenomena and potential applications for such hybrid materials.[141]

3.2.2 MOF-based luminescent sensing for VOCs. LMOFs combine the general advantages of MOFs (porosity, tailorability, *etc.*) with their inherent luminescent properties, making them interesting for sensing applications. The luminescent sensing is essentially based on the host–guest interactions between the analytes molecules and the LMOFs, which gives rise to variations in the luminescent intensity (*e.g.* turn-on and turn-off effects) or peak positions. Classic sensing mechanisms are photo-induced electron transfer (PET), intermolecular charge transfer (ICT) and Förster energy transfer (FRET).[24,152] A detailed description of every sensing mechanism in LMOFs can be found in the reviews by Yan,[153] while Cui *et al.* specifically focused on

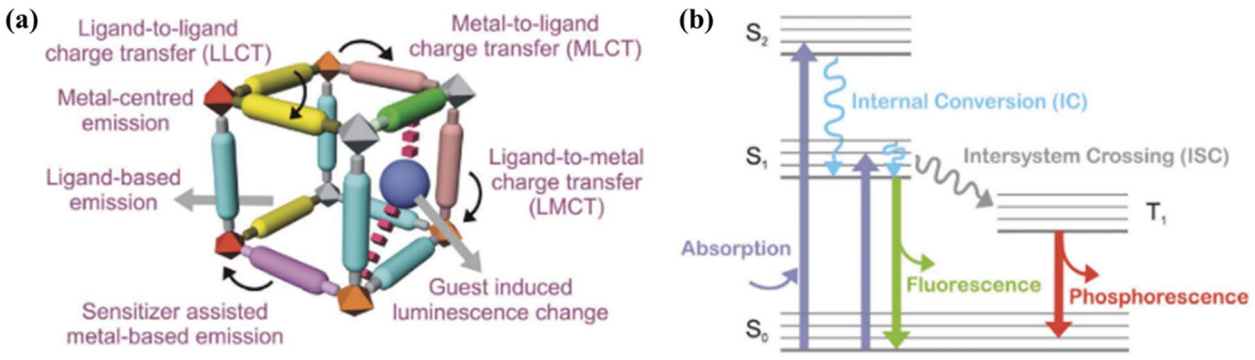

Fig. 6 (a) Schematic diagram of various origins of luminescence in LMOFs. (b) Illustration of photon emission in ligand-centred luminescence. Adopted from ref. 151.

Open Access Article. Published on 05 lokakuuta 2022. Downloaded on 8.6.2026 20.57.17.
This article is licensed under a Creative Commons Attribution-NonCommercial 3.0 Unported Licence.

sensing strategies with potential in practical applications, which include the use of functional sites for selective sensing, turn-on luminescent sensing and self-referencing sensing based on dual-emitting MOFs.[149] It is noteworthy that LMOFs also bear limitations such as relatively low sensitivity compared to organic based systems when the sensitivity comes from ligand-to-metal-transfer.

LMOF-based gas/vapour sensing has been extensively investigated and comprehensively reviewed recently.[141,149,151,152,154–159] Similar to chromism-based sensing, finely tuning the physical and chemical properties of LMOFs, such as introducing functional groups, tuning the hydrophobicity/hydrophilicity, the Lewis acidity/basicity, or adjusting the steric hindrance effect, can improve selectivity.[24,160] Li *et al.* provided their comprehensive insights on the rational designs of LMOFs as functional chemosensors, along with notable considerations of practical parameters for seeking real-time applicability. They also extensively reviewed the progress of LMOFs as explosive sensors, humidity sensors, gas sensors, ion sensors and VOC sensors.[151] Another review published later by the same group highlighted the detection of different types of VOCs, chemical warfare agents and hazardous gases.[158] Sensing of environmental pollutants including pesticides, antibiotics, heavy-metal-ions, explosives and VOCs using LMOFs has also been highlighted.[152,159] Reviews by Lin *et al.*[156] and Khatua *et al.*[157] also highlighted the advantages of using flexible LMOFs in gas/vapour sensing applications. Recently, Yao *et al.* grafted a non-planar organic chromophore, 3-TPPA (tri(4-(pyridine-3-yl)phenyl)amine (3-TPPA)), into a 2D flexible MOF, MOF-105, *via* one-pot synthesis and realized a wide range of emission colour tuning[107] (Fig. 7a). The bulk crystal of the free-standing 3-TPPA chromophore exhibited only emission intensity changes at different temperatures. However, the resulting hybrid material emission can be modulated by both temperature and pressure stimuli as well as VOC sorption *via* positive (solvato-)fluoro–chromism interactions.

With the rapid growth of LMOF-based sensing, new mechanisms and platforms are also emerging. In 2020, Liu *et al.* designed and synthesized a rigid Cu(I)-based MOF $[Cu_4I_4(Py_3P)_2]_n$ (Py_3P = tris(2-pyridyl)phosphine) that displayed a guest-induced luminescence enhancement mechanism.[108] Upon exposure to chlorinated VOC vapours (CH_2Cl_2, $CHCl_3$ and $C_2H_4Cl_2$), a turn-on detection mode was observed with an obvious enhancement of luminescence intensity, compared to other VOC vapour exposures such as benzene, CH_3OH, acetone and DMF. The weak host–guest interactions between chloroalkane molecules and the host framework decrease the molecular vibrations inside the MOF, resulting in luminescence enhancement (Fig. 7b). In the same year, the first report on enhanced fluorescence of self-assembled colloidal crystal films was achieved by Olorunyomi *et al.* They incorporated the fluorescent dye Nil red (NR) into ZIF-8 colloidal crystals, followed by self-assembly of dye-functionalized MOF particles into colloidal crystal films *via* dip-coating.[109] The periodically ordered assembly of NR∼ZIF-8 colloidal crystals (denoted as NR∼*cc*ZIF-8 films) enhanced the fluorescence by 186 fold compared to disordered samples. Furthermore, the NR∼*cc*ZIF-8 films respond to different organic vapours (acetone, methanol, toluene and xylenes) at various concentrations *via* fluorescent quenching. The highest response was obtained with toluene vapours, whereas the lowest occurred from xylene isomer exposure. The selectivity is evoked from molecular size and shape exclusion, which indicates the importance of porosity in colloidal crystal assemblies for fluorescent sensing.

Despite advancements in LMOFs for sensing applications, further improvements are still required for the practical implementations of LMOFs in sensors: (1) in the aspect of sensing VOCs, the majority of the reported results were

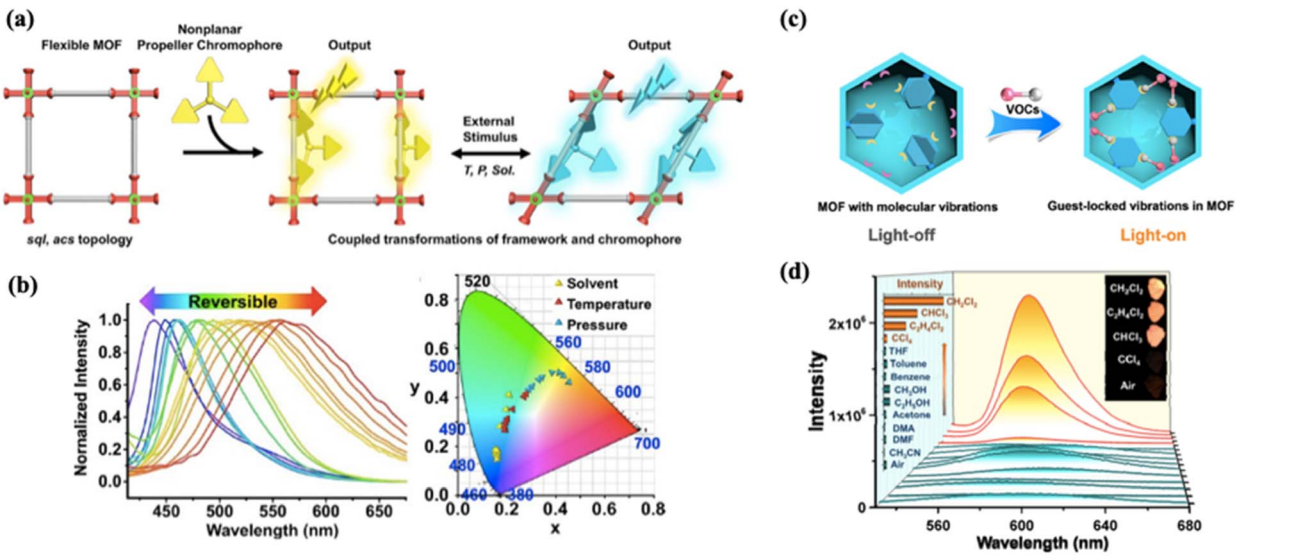

Fig. 7 (a) Illustration of the organic chromophore 3-TPPA grafted in the dynamic coordination space of a flexible MOF. (b) Wide-range emission colour tuning of a 3-TPPA grafted MOF-105 material.[107] (c) Illustration of the guest-induced luminescence enhancement mechanism in the presence of VOCs. (d) Emission spectra of $[Cu_4I_4(Py_3P)_2]_n$ after incubation for 30 min in various solvent vapours.[108]

© 2022 The Author(s). Published by the Royal Society of Chemistry

Open Access Article. Published on 05 lokakuuta 2022. Downloaded on 8.6.2026 20.57.17.
This article is licensed under a Creative Commons Attribution-NonCommercial 3.0 Unported Licence.

examined in the liquid phase, yet the response might differ when the material encounters vapour-phase analytes. (2) The dominant construction strategy of LMOFs relies on either lanthanide metal ions or bulky π-conjugated ligands, which generally are costly and produced on small scales. The typical synthesis of LMOFs highly depends on solvothermal reactions. Thus, scale-up synthesis and stability of LMOFs on a longer time scale still await further examination. (3) The luminescent responses are, mostly, changes in emission intensity and positions, which are currently measurable through laboratory instruments. The signal transduction can therefore not be trivial, and the material needs to be first coupled with electronics with proper shaping processes. (4) Shaping of LMOFs is also an important step toward practical applications, and it calls for further attention, as it is another concern for fabricating a luminescent sensing device. In conclusion, luminescent MOFs for gas/vapour sensing application are still a young and active field with many promising results and several opportunities remain to move LMOFs from lab-scale to real-world applications.

3.3 Sensors based on optical index modulation

3.3.1 Fabry–Perot interferometers. Interferometry is a technique based on the interaction between waves.[161] Fabry–Perot interferometers, also known as etalons, typically utilize the reflections and transmissions between two closely seated parallel reflective surfaces. When the incident light travels in the cavity, multiple reflections occur and the path-length difference between subsequent transmissions results in an interference pattern, as shown in Fig. 8.[162] The intensity of the output interference pattern is highly dependent on the distance between the mirrors l. When the distance l equals half of the wavelength of the incident light λ or one of its multiples, a standing wave with the longitudinal mode is created and a maximum transmittance is observed at the detector. The following equation can express this correlation:

$$\lambda = \frac{2nl}{m}$$

where m is the number of half wavelengths inside the cavity and n is the refractive index of the active medium.

MOF films can function as the responsive medium of the Fabry–Perot (F–P) cavity. The first proof of concept was described by Lu and Hupp in 2010 for selective sensing of chemical vapours.[163] For example, a transparent thin film of ZIF-8 was deposited on an appropriate substrate (glass or silicon) and films with different thicknesses exhibited various colours, which can be attributed to the thickness-dependent optical interference in the visible region. Given that the cavity of ZIF-8 is evacuated and under vacuum ($n_{vac} = 1$), absorption of guest molecules modifies the bulk refractive index of the MOF, and red-shifts the interference peaks accordingly. In 2016, Chen *et al.* presented a high-performance etalon composed of hollow ZIF-8 nanoshell arrays and a thin layer of Pt coating, named a hollow MOF nanoshell-based etalon (HMNSE).[110] The hollow ZIF-8 arrays function as the dielectric medium in between the reflective Si wafer substrate and the metal layer. The fabrication of the device requires several steps including repetitive *in situ* growth of ZIF-8 on a monolayer of polystyrene (PS) nanospheres, removal of the PS cores to form the hollow structure of the MOF, followed by sputtering of Pt (Fig. 9a). The interference peak wavelength and accordingly the colour of HMNSE were tuned by varying the size of the ZIF-8 shell. Such construction allows large optical response and distinct colour outputs for selective detection of alcohols, ketones, nitriles, cyclohexane/benzene and xylene isomers in the vapour phase, as well as good repeatability and recyclability. Fig. 9 presents the sensor optical shift upon exposure to saturated acetonitrile vapour (b) and different alcohols (c). This device also exhibits a wide detection range from 1000 to 20 000 ppm for acetone vapours with a good correlation between the wavelength shift and the vapour concentration. Zhang *et al.* have also reported a Fabry–Perot optical sensor based on self-assembled UiO-66 nanocrystals for VOC vapour sensing. They demonstrated that controlling the size and the missing-linker amount in UiO-66 crystals can tune the optical properties of the film, as well as enhance the sensitivity and recovery performance of the sensor.[164] Recently, Li *et al.* encapsulated TiO_2 nanoparticles in

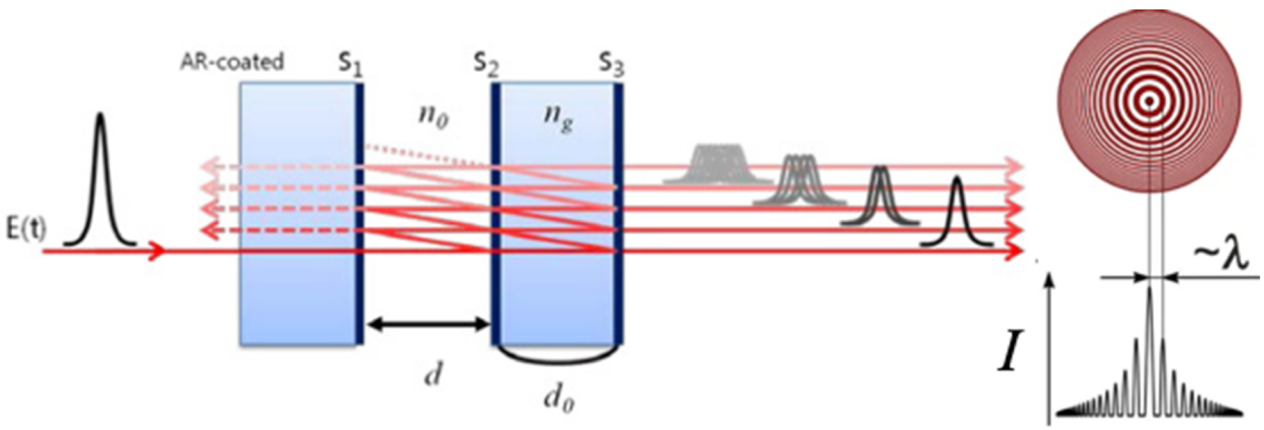

Fig. 8 Illustration of the working principle of a Fabry–Perot interferometer and a typical Fabry–Perot interference pattern.

Open Access Article. Published on 05 lokakuuta 2022. Downloaded on 8.6.2026 20.57.17.
This article is licensed under a Creative Commons Attribution-NonCommercial 3.0 Unported Licence.

an HKUST-1 thin film in order to improve the sensitivity and response time of the sensor.[111] The HKUST-1⊃TiO_2 composite film was fabricated through the layer-by-layer deposition of spray-coated MOF precursor solutions and pre-synthesized TiO_2 NP solution alternatively (Fig. 9d). The authors demonstrated that the incorporation of TiO_2 NPs increases the optical quality of the film, with narrower reflection bands and more intense reflectance compared to a bare MOF film of similar thickness. Furthermore, TiO_2 NPs brought a higher affinity to isopropanol, ethanol and methanol for the HKUST-1-based F–P cavity, which was revealed by a larger redshift of the reflection bands upon vapour exposure. A shorter response time (27.6 s for HKUST-1 *vs.* 12.6 s for HKUST-1⊃TiO_2 to acetone) was also observed with the HKUST-1⊃TiO_2 composite due to enhanced H-bonding between TiO_2 NPs and the tested oxygen-containing molecules.

Colloidal crystals are typically submicron-sized spheres of silica or polymers in an ordered arrangement. The periodic

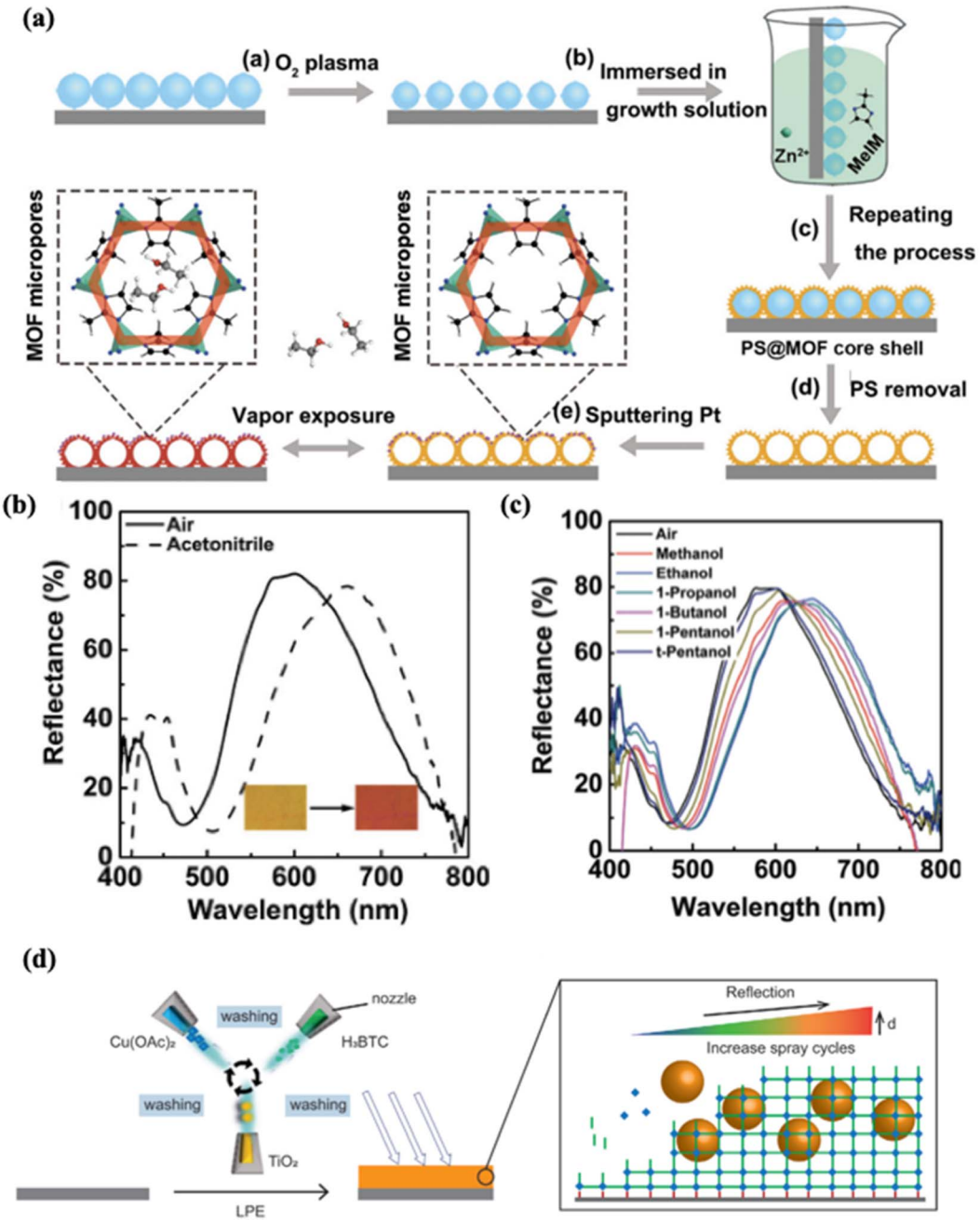

Fig. 9 (a) Illustration of the experimental procedure used to fabricate a HMNSE. (b) HMNSE with 2 nm Pt coating before and after exposure to saturated acetonitrile vapour at 293 K. The insets show the corresponding optical microphotographs. (c) Optical response of the HMNSE to different alcohols, including methanol, ethanol, 1-propanol, 1-butanol, 1-pentanol, and *tert*-pentanol.[110] (d) Schematic of the liquid phase epitaxy (LPE) method for sequential TiO_2-loading in MOF films.[111]

© 2022 The Author(s). Published by the Royal Society of Chemistry

Open Access Article. Published on 05 lokakuuta 2022. Downloaded on 8.6.2026 20.57.17.
This article is licensed under a Creative Commons Attribution-NonCommercial 3.0 Unported Licence.

variation of the refractive index in the crystals enables them to reflect light at a specific wavelength, also known as a stopband. Adsorption of guest molecules can shift the stopband due to the changes in their effective refractive indices and/or lattice spacing.[165] Based on this strategy, Hupp *et al.* have shown that coating a thin layer of ZIF-8 on colloidal crystals (CCs) can give rise to a device capable of VOC sensing.[165] Li *et al.* also managed to deposit an ultrathin layer (~80 nm) of ZIF-8 on monolayer colloidal crystals (MCCs) *via* the LBL method.[166] This sensor can discriminate between different alcohols *via* the colorimetric response together with shifts in the reflectance peak. Later on, Chen *et al.* fabricated another optical sensor based on the self-assembly of polyhedral ZIF-8 into MCCs.[112] Three polyhedral ZIF-8 particles with different exposed facets were assembled, namely truncated cubic (TC) ZIF-8, truncated rhombic dodecahedral (TRD) ZIF-8, and rhombic dodecahedral (RD) ZIF-8 (Fig. 10a–d). A thin layer of Pt was sputtered on the MOF layer to enhance the output signal, leading to narrower full width at half maxima (FWHM), higher reflectance peaks to valley ratios (p–v ratios) and more vivid colours (Fig. 10e–f). Compared to polycrystalline ZIF-8, RD ZIF-8 MCCs lead to a more controlled crystal orientation and elimination of grain boundaries, resulting in a refined selectivity towards linear olefins (*e.g.* 1-hexane) over other BTEX species (benzene, toluene, ethylbenzene and xylene). Furthermore, the authors demonstrated that different exposed facets of ZIF-8 can regulate the sensitivity of the sensor *via* differentiated diffusion (Fig. 10h). Specifically, exposing the (110) facet of ZIF-8 allows a more completed exposure of the six-membered window and consequently realizes the detection of C1–C8 linear alcohols, as well as the colorimetric discrimination of C5–C8 alkanes (Fig. 10g).

3.3.2 Bragg stacks. Bragg stacks (BSs), also known as Bragg mirrors or one-dimensional photonic crystals (1D PCs), typically consist of multiple dielectric layers with alternating high- and low refractive indices (RI). The periodic structure enhances the reflections of certain wavelengths because of the diffraction and interferences at every interface.[113,167–169] The optical response can often be intrinsically tuned by modifying the incident

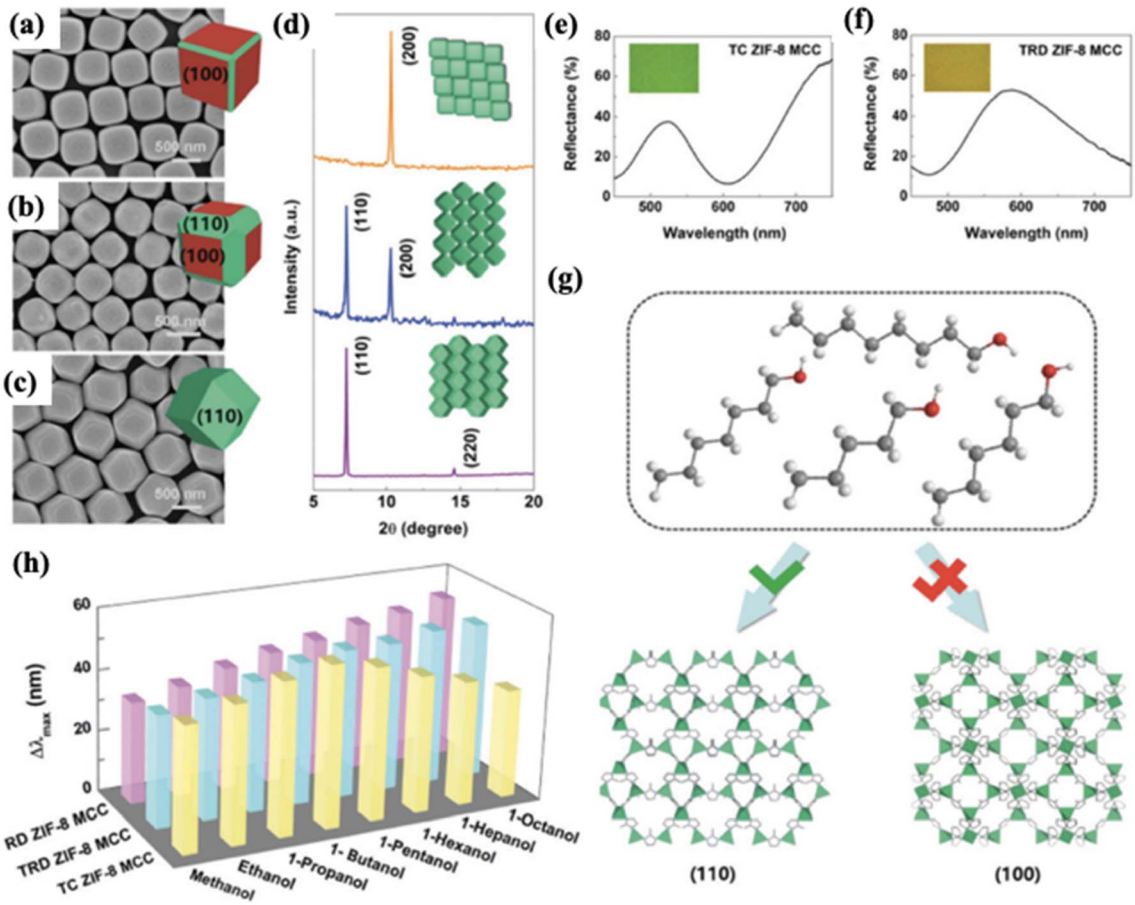

Fig. 10 (a)–(c) SEM images of ZIF-8 MCCs of different crystal morphologies: TC ZIF-8 (a), TRD ZIF-8 (b) and RD ZIF-8 (c). The insets show schematic representations of the corresponding crystal morphologies. (d) PXRD patterns of ZIF-8 MCCs of different crystal morphologies showing preferential orientations. The insets show schematic representations of the corresponding arrangement of ZIF-8 nanoparticles. From top to bottom: TC ZIF-8, TRD ZIF-8 and RD ZIF-8. (e) and (f) Reflectance spectra of TC ZIF-8 MCCs (e) and TRD ZIF-8 MCCs (f). The insets show the corresponding optical micrographs. (g) Schematics showing the adsorption of C5–C8 linear alcohols on ZIF-8 through (110) and (100) planes. (h) $\Delta\lambda_{max}$ of ZIF-8 MCCs of different crystal morphologies in response to C1–C8 linear alcohols: RD ZIF-8 (pink), TRD ZIF-8 (cyan) and TC ZIF-8 (yellow).[112]

Open Access Article. Published on 05 lokakuuta 2022. Downloaded on 8.6.2026 20.57.17.
This article is licensed under a Creative Commons Attribution-NonCommercial 3.0 Unported Licence.

angles[170] and the stack thickness.[113,114] Similar to F–P interferometers, the position of the diffraction maxima λ_{max} is at normal incidence and is given by:[113,114]

$$\lambda_{max} = \frac{2(n_H l_H + n_L l_L)}{m}$$

where the indices H and L represent the high- and low-RI layer, respectively. In MOF-based BSs, MOFs typically function as the low-RI layers and TiO_2 (ref. 113, 114 and 170) or polymers[168] are often employed as the high-RI layers. Adsorption of guest molecules varies the refractive index of the MOF layers (n_L) and accordingly shifts the reflectance peaks. Selectivity can be achieved *via* size sieving, pore accessibility and/or host–guest interactions between MOFs and the analytes.

The first MOF-based Bragg stack based on ZIF-8 and TiO_2 for ethanol sensing was introduced by Lotsch *et al.*, where ZIF-8 functions as the low-RI layer and TiO_2 possesses a high RI.[169] Patterning of ZIF/Pt BSs[171] and 3D-ordered MOF photonic films[172] for sensing application has also been achieved. BSs were also prepared with NH_2-MIL-88 for selective sensing of EtOH vapour, benefitting from the selective breathing behaviour of MIL-88.[170] Lotsch *et al.* also assembled an optical sensor array from three TiO_2/MOFs BSs (TiO_2/ZIF-8, TiO_2/HKUST-1, and TiO_2/CAU-1-NH_2).[113] Combining responses from multiple MOF elements with appropriate signal analysis methods (colour image analysis and principal component analysis-PCA) generated analyte-specific fingerprints, which facilitated the single component discrimination of mixed vapours. In another study by the same group, post-synthetic modification (PSM) on either the SBU or the linker of CAU-1(Al) directly on an assembled BS of TiO_2/CAU-1 was achieved to precisely tune the sensitivity and selectivity of the active MOF layers.[114] De-methoxylation of the SBU increased the pore accessibility and improved the possibility to form hydrogen bonds, while amidification of the linker with hexanoic acid brought hydrophobicity. Both modulations allowed a better distinction among water, alcohols (methanol, ethanol and iso-propanol) and *n*-heptane vapours. The first Bragg stack composed of NH_2-MIL-88B nanoparticles and a functional polymer poly(styrene-acrylic acid) was reported in 2020.[168] The polymer and the flexible MOF can both undergo swelling upon BTEX sorption and the associated volume change induces modifications in the thickness and RI of both components. Consequently, the sensitivity of the sensor is boosted with contributions from both parts. The brown-purple film also exhibited a colour variation correlated to the concentration of exposed BTEX vapours. Selective sensing of chlorobenzene has also been achieved using two other strategies: combining MOFs and graphene oxide as the sensing layer[173] and MOF metal doping.[174]

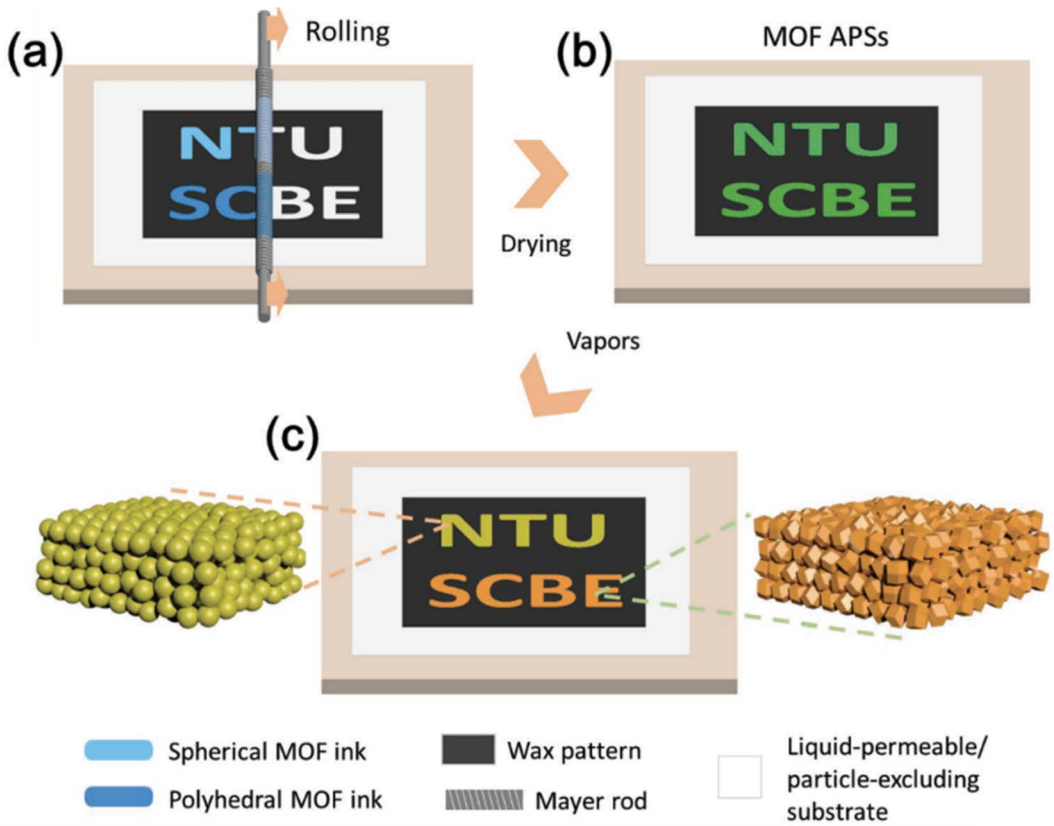

Fig. 11 Illustration of Mayer rod coating of a MOF amorphous photonic structure (APS). (a) Selective wetting of the hydrophilic area of the substrate during coating with spherical/polyhedral MOF inks; (b) formation of APS patterns of spherical or polyhedral MOF particles after the removal of water; (c) vapour-responsive colour changes of the MOF APS patterns.[175]

© 2022 The Author(s). Published by the Royal Society of Chemistry

Open Access Article. Published on 05 lokakuuta 2022. Downloaded on 8.6.2026 20.57.17.
This article is licensed under a Creative Commons Attribution-NonCommercial 3.0 Unported Licence.

3.3.3 Diffraction grafting and colloidal film engineering. Engineering colloidal films of MOFs can create photonic structures for sensing applications. For example, Faustini *et al.* have described a soft-lithographic technique for the fabrication of sub-micrometer 2D photonic structures based on colloidal ZIF-8 or ZIF-8/TiO_2 nanocomposites.[115] The sensor presented a selective detection of styrene under the interference of humidity, with a LoD of 57 ppm. The signal was transduced by the change in colour luminance, which originated from the MOF refractive index variation upon adsorption of the targeted analytes and can be detected by using integrated cameras in smartphones. The same group also demonstrated an evaporation-directed crack patterning of MIL-101(Cr) colloidal films.[116] The crack pattern was promoted during dip-coating deposition, where controlling the evaporation front and the withdrawal speed guided the crack propagation and periodicity differently. The crack arrays acted as diffraction grafting and allowed the detection of toluene down to 200 ppm. Bai *et al.* introduced a responsive amorphous photonic structure (APS) constructed by the colloidal assembly of spherical/polyhedral ZIF-8 particles on a liquid-permeable substrate.[175] The infiltration-assisted Mayer rod coating can customize the colour of the film by controlling the wetting process (see Fig. 11). This photonic structure exhibited a vapour-responsive colour variation, where distinctions among ethanol, methanol, acetone, toluene and DMF can be realized.

3.3.4 Optical fibres. Optical fibres are often made of silica or plastic for the core, covered by a cladding layer with a lower refractive index. This structure allows light to propagate along the fibre by total internal reflections (TIRs), where the fibre acts as a waveguide. In such a manner, light can be transmitted over long distances with low loss and immunity to electromagnetic interferences. Optical fibres are commonly employed in telecommunication, but they have also been explored as chemical sensors. Fibre optic interferometry is one of the chemical sensing approaches that makes use of optical fibres and is known for its high sensitivity, but lacks chemical specificity.[162] One solution is to combine MOF nanocrystals with optical fibres for improved selectivity. Several MOF-coated optical fibres have been reported to be able to selectively detect CO_2 and H_2.[176–179] Some studies have also explored their potential for VOC sensing. For example, Zhu and coworkers coupled a single crystal of HKUST-1 to the end-face of an optical fibre using epoxy glue for quantitative detection of nitrobenzene

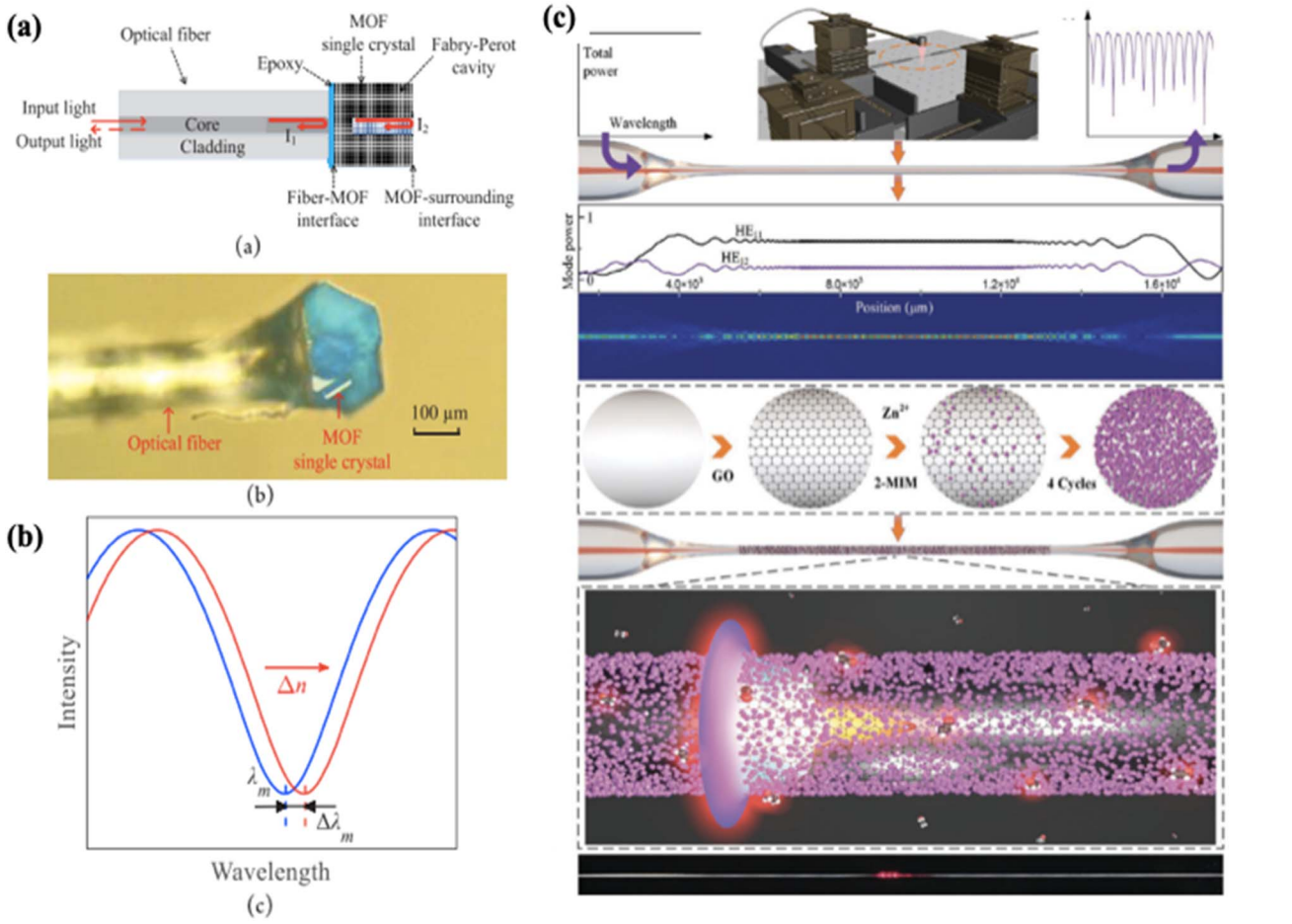

Fig. 12 (a) Schematic diagram of the HKUST-1 coated optical fibre sensor and an optical microscope image of the sensor. (b) Illustration of a section of the original (blue) and shifted (red) interferograms.[180] (c) Schematics of the modification step at the interface of the optical microfibre with a ZIF-8/GO functional layer.[118]

Open Access Article. Published on 05 lokakuuta 2022. Downloaded on 8.6.2026 20.57.17.
This article is licensed under a Creative Commons Attribution-NonCommercial 3.0 Unported Licence.

(Fig. 12a).[180] The sensing mechanism is based on the variation of the refractive index induced by the adsorption of nitrobenzene within the MOF crystal. The quantification was achieved by analysing the shifts of the interference spectra derived from the fibre optic interferometry (Fig. 12b). Cao *et al.* also developed a methane-sensitive cladding layer by integrating ZIF-8 into a UV-curable polymer.[181] The detection limit of 1% methane in nitrogen was achieved by employing the ZIF-8/polymer coating in either single-mode or multi-mode fibres. In another study, Chen *et al.* realized the on-chip integration of ZIF-8 on the surface of a SiO_2 waveguide.[117] The fabricated sensor exhibited high sensitivity towards ethanol with a large detection range of 0–1000 ppm and a low detection limit of 1.6 ppm. Recently, Huang *et al.* fabricated an optical microfibre interferometric VOC sensor based on evanescent field interaction with ZIF-8/graphene oxide nanocoating.[118] The surface of the optical fibre was pre-modified with graphene oxide (GO), where multilayers of ZIF-8 were grown subsequently *via in situ* synthesis (Fig. 12c). The GO layer enhanced the adhesion and homogeneity of ZIF-8 layers due to the large π-conjugated network of GO. The sensor presented an ultrafast response of 118 ms towards ethanol with a LoD of 5.26 ppm, which was attributed to the porous structure of the ZIF-8/GO composite.

Long-period grafting (LPG) optical fibres are another well-known type of sensor that relies on the modulation of refractive indices. Typically, a periodic perturbation of the refractive index is present on an LPG fibre, which results in a series of attenuation bands in the transmission spectrum. Each band corresponds to different couplings between the core mode and a particular cladding mode. As such, the exposure of guest vapours induced changes in the refractive index of the cladding that shifted the attenuation band.[162,182–184] Hromadka *et al.* have reported a LPG-based sensor working at a phase-matching turning point presenting a high sensitivity for ethanol and acetone.[184,185] In another study, Chiang *et al.* developed a fibre interferometer with a pair of cascaded LPGs, where ZIF-8 was coated on the surface of the cladding.[119] The LPGs enable a co-propagating mode, where the light in the core and the cladding interfere with each other and results in a sharp interference fringe as shown in Fig. 13. Ethanol and methanol showed the largest interfering fringe shifts and greatest RI changes from 1.216 to 1.499 and 1.476, respectively. DFT calculations attributed the distinctive responses toward ethanol and methanol to their different desorption energies from ZIF-8. In a follow-up study, Chiang *et al.* utilized the same configuration for real-time monitoring of bulkier molecules (*e.g.* toluene and pyridine) and proved that the adsorption dynamics is greatly linked to molecular geometries and kinetic diameters of the guest molecules.[183] Adsorption of toluene on ZIF-8 shifted the outcome interference spectrum by 4.3 nm after 40 min of exposure. However, due to the slow adsorption dynamics and difficulty in desorption, the device is rather suitable for toluene capture than for the sensing application.

3.3.5 Micro-ring resonators. Similar to optical-fibre-based sensors, photonic micro-ring resonators detect the analytes based on evanescent field interaction and consequent changes in the refractive index. However, the waveguides, in that case, are bendable and connected in a closed loop with a light source and a detector. Light in micro-ring resonators is propagated in the fashion of a circulating waveguide mode, which is derived from the total internal reflection of an arced boundary between a high and a low refractive index medium. As a result, the interaction between the sensitive layer and the analytes gives rise to a shift in the resonant wavelength.[21,29] Tao *et al.* exemplified a micro-ring resonator with ZIF-8 coating for detection of multiple VOCs at the ppb level including styrene, toluene, benzene, propylene and methanol.[29] The coating of ZIF-8 was achieved by *in situ* growth followed by chemical etching. In the presence of ZIF-8, the sensitivity of the resonator was enhanced by a factor of up to 1000 for propylene compared to that of

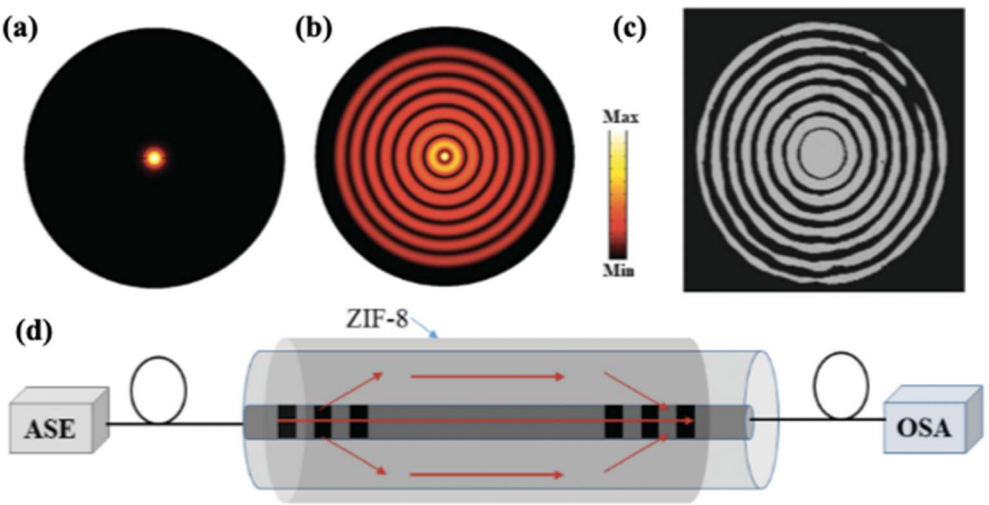

Fig. 13 (a) Optical power distribution of the fundamental mode (LP_{01}, core mode) and (b) higher-order mode (LP_{08}, cladding mode); (c) near-field image of the LP_{08} mode pattern obtained with an infrared camera; (d) schematic diagram of the proposed fibre interferometer with cascaded LPFGs. ASE: amplified spontaneous emission light source; OSA: optical spectrum analyzer.[119]

© 2022 The Author(s). Published by the Royal Society of Chemistry

Open Access Article. Published on 05 lokakuuta 2022. Downloaded on 8.6.2026 20.57.17.
This article is licensed under a Creative Commons Attribution-NonCommercial 3.0 Unported Licence.

a bare resonator. This can be attributed to the preconcentration of the analytes in ZIF-8. In addition, the hydrophobicity of ZIF-8 also made the device much less sensitive to humidity. The LoD ranged from 29 to 99 ppb with a response time of 30 min, which can be suitable for applications requiring high-accuracy.

3.3.6 Surface plasmon resonance. Surface plasmon resonance (SPR) occurs when incident light stimulates the resonant oscillation of plasmons at the interface between two media with opposite permittivity. When plasmonic metal nanoparticles are involved, the nanoscale dimension confines the oscillation on the particle surface, which is known as localized surface plasmon resonance. Plasmonic nanoparticles, typically Ag, Au and Cu, can interact with light in the visible and near-infrared regions. The presence of analytes at their surface can modify the local RI and results in a shift in the resonance wavelength. MOFs incorporating SPR platforms can amplify the sensor response, therefore extending its applications from biomolecule detection to VOC sensing.[186,187]

Vanderzande *et al.* presented a ppm-level detection of alcohol vapours using MOF-functionalized SPR sensors.[120] A layer of ZIF-8 or ZIF-93 was deposited as a recognition layer on a gold surface of fibre-optic-based SPR sensors (see Fig. 14a). Upon exposure to several alcohol vapours (MeOH, *n*-BuOH, *etc.*), the bare SPR sensor did not exhibit any detectable SPR activity due to the low intrinsic RI of the alcohols. With the assistance of MOF coating, vapours with ppm concentrations were detected. A LoD of 2.5 ppm for methanol was realized by the ZIF-8 coated sensor. ZIF-93 coating presented the highest sensitivity and selectivity towards MeOH at low partial pressure due to its hydrophilicity, whereas ZIF-8 showed high sensitivity to MeOH at high partial pressure because of the molecular clustering effect. Such differences in recognition behaviour can be used for qualitative distinction of the vapour composition. Recently, Ameloot *et al.* explored surface plasmon polariton (SPP) resonance by incorporating a ZIF-8 thin film *via* the CVD approach onto an AlO_x/Ag layered surface on a glass substrate for methanol detection.[121] The sample configuration is illustrated in Fig. 14b. The signal of VOC uptake was transduced into SPP shifts by applying spectroscopic total internal reflection ellipsometry (TIRE). Upon exposure to MeOH vapour, the sensor responded up to 160 nm in the SPP shifts with a LoD lower than 1 ppm (Fig. 14c). A resolution of 10^{-5} in refractive index units was achieved by optical modelling of measured TIRE/SPP spectra, which outperformed conventional ellipsometric porosimetry.

3.3.7 Surface-enhanced Raman scattering. Surface-enhanced Raman scattering is an ultrasensitive vibrational spectroscopic analytical technique. It is based on the working principle of traditional Raman spectroscopy that identifies and quantifies the analytes with their characteristic vibrational fingerprints. Enhancement of Raman signals is achievable by adopting SERS-active substrates such as plasmonic particles,

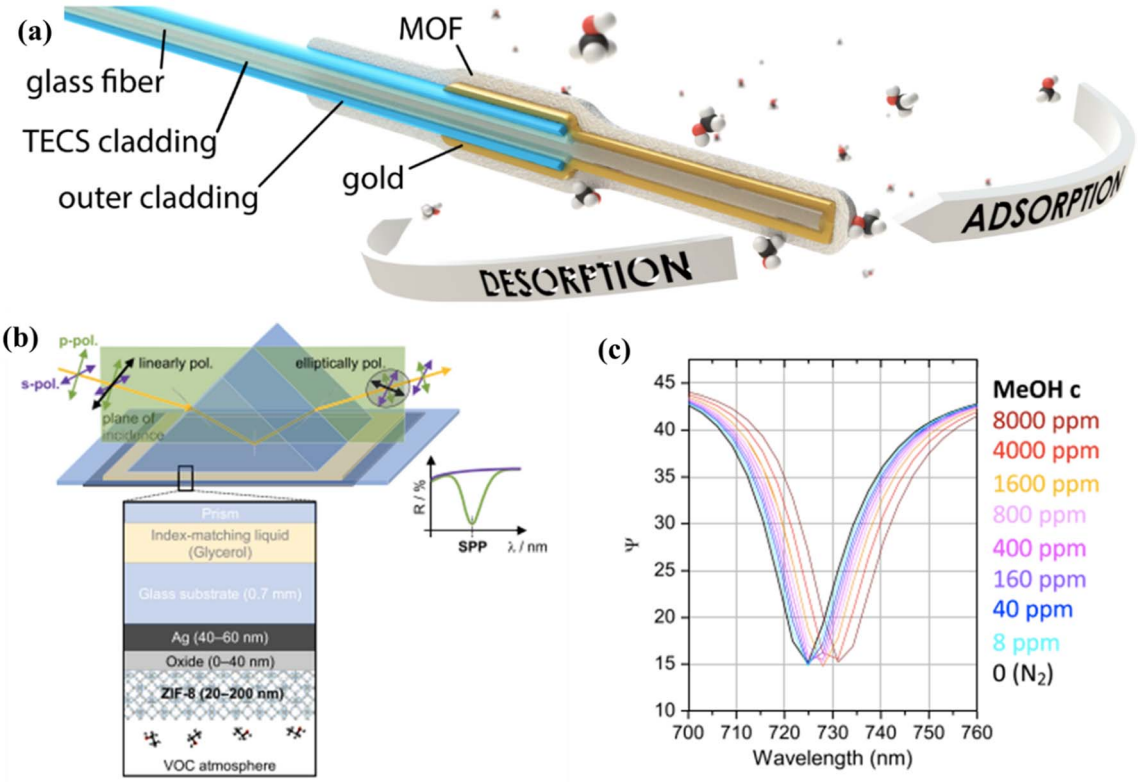

Fig. 14 (a) Schematic representation of an MOF-FO-SPR probe (not at real scale). The probe consists of an optical fibre with a diameter of 400 μm with the inner TECS cladding and the outer protective cladding removed from the end. A gold layer is covered with a MOF which functions as a recognition layer. The atoms in the floating methanol molecules are oxygen (red), carbon (black), and hydrogen (white).[120] (b) TIRE/SPP principle and TIRE measurement geometry with the sample layer stacks. (c) The measured SPP peak redshift in methanol compared to dry N_2.[121]

Open Access Article. Published on 05 lokakuuta 2022. Downloaded on 8.6.2026 20.57.17.
This article is licensed under a Creative Commons Attribution-NonCommercial 3.0 Unported Licence.

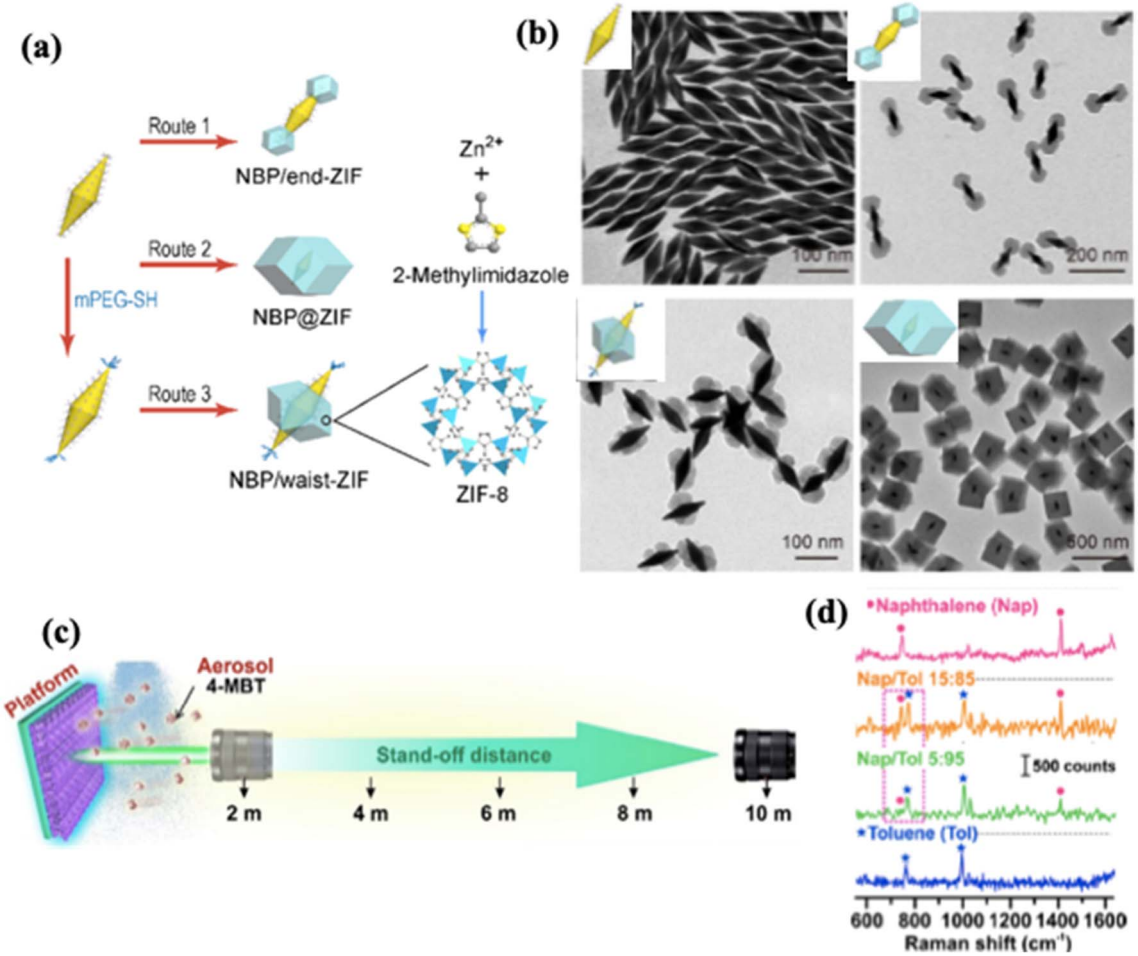

Fig. 15 (a) Schematics of the routes for selective deposition of ZIF-8 on the Au NBPs. (b) TEM images of the Au NBPs, NBP/end-ZIF, NBP/waist-ZIF, and NBP@ZIF nanostructures, respectively.[194] (c) Illustration of the setup for stand-off SERS sensing. (d) Stand-off multiplex spectra obtained under outdoor conditions with natural light, for two different mixtures of naphthalene and toluene, with reference to individual naphthalene and toluene SERS spectra.

for instance Au and Ag, which can generate an enhanced electromagnetic field on the surface upon excitations and accordingly amplify the signals. The poor affinity between the plasmonic surface and analytes is often addressed as a problem with SERS platforms. Incorporating MOFs with SERS essentially facilitates the selectivity and sensitivity by preconcentrating the analytes and introducing intermolecular interactions between the framework and guest molecules.[188–190]

Koh *et al.* reported a plasmonic nose by encapsulating Ag nanotubes in ZIF-8 (Ag@ZIF-8) for molecular-level recognition of VOCs.[122] The combination of Ag and ZIF-8 leads to preconcentration of analyte molecules and enhancement of the electromagnetic (EM) field at the nanoscale. The ultra-trace SERS detection of VOCs was facilitated by optimizing the thickness of the ZIF-film for maximizing the volume of preconcentrated vapour and tailoring the plasmonic coupling between neighbouring Ag nanotubes to intensify the EM hotspots. The Ag@ZIF-8 plasmonic nose exhibited a SERS response towards multiple vapours including toluene and chloroform. Specifically, it presented unique vibrational features for toluene down to 200 ppm and a linear quantification of toluene in the range from 200 to 2000 ppm. Osterrieth *et al.* fabricated a core–shell structure of Au nanorods (Au NRs) and Zr-MOFs NU-901 for SERS detection of thiolated analytes.[191] NU-901 is composed of eight-connected Zr_6 oxoclusters and tetratopic 1,3,5,8-(*p*-benzoate)pyrene linkers (H4TBAPy). The 1D diamond-shaped channel of NU-901 has the dimension of *ca.* 12 × 26 Å which allows fast diffusion of relatively large analytes. Au NRs as seeds facilitated the MOF growth at room temperature with a core–shell structure and a yield higher than 99% under optimal conditions. The composite maintained the SERS capability of the Au NRs, allowing the selective adsorption and detection of thiolated polystyrene with SERS spectra. In other examples, Li *et al.* constructed core–shell HKUST-1@Ag NPs *via in situ* electrodeposition for SERS detection of polycyclic aromatic hydrocarbons[192] and Chen *et al.* achieved SERS detection for toluene, ethylbenzene, and chlorobenzene by constructing a similar core–shell structure of Au@ZIF-8.[193] Another platform of Au@Ag nanorods encapsulated in ZIF-8 was fabricated by Lafuente *et al.* for chemical warfare agent

© 2022 The Author(s). Published by the Royal Society of Chemistry

Open Access Article. Published on 05 lokakuuta 2022. Downloaded on 8.6.2026 20.57.17.
This article is licensed under a Creative Commons Attribution-NonCommercial 3.0 Unported Licence.

detection in ambient air.[123] Yang *et al.* also demonstrated a site-selective deposition of ZIF-8 on Au nanobipyramids for SERS detection of toluene and aniline vapours.[194] ZIF-8 was selectively grown either at the ends, at the waist, or by forming a core–shell structure on the bipyramids. The formation of the selectively deposited ZIF-8 was confirmed by SEM and TEM images shown in Fig. 15a and b. All three nanostructures presented distinctive Raman peaks of toluene and aniline under the vapour exposure, indicating the occurrence of analyte interactions with the MOF. The end-deposited Au NBP@ZIF-8 presented the strongest Raman signals, which can be explained by the large local electric field at the sharp ends of the Au NBPs.

Phan-Quang *et al.* also realized real-time stand-off SERS spectroscopy with the integration of Ag@ZIF-8 for remote and multiplex detection of airborne molecules.[124] The platform was fabricated *via* drop-casting multiple layers of the solution of a pre-synthesized Ag@ZIF-8 core–shell composite. The formed 3D structure of Ag@ZIF-8 has a thickness of *ca.* 1.3 μm after 10–15 layers with an interparticle distance of Ag cores of *ca.* 10 nm, which allows strong plasmonic coupling for intense SERS hotspots. Upon exposure to vapours of the probe molecule 4-methylbenzenethiol (4-MBT), it presented a rapid response of 10 s at 500 ppm and the signals were 6-fold more intense compared to those of the control platforms (the MOF-coated Ag platform and bare Ag nanocubes). Notably, the multilayered structure also brought an appropriate hotspot focal depth to be able to cooperate with the stand-off Raman system. The response of the sensor can therefore be recorded with a detector placed 2–10 m apart with 8-fold less laser power employed (≤55 mW, see Fig. 15c). The Ag@ZIF-8 combined stand-off Raman detection can respond to a minimum of 50 ppb aerosolized 4-MBT and a linear calibration curve can be constructed within the range of 500 ppm to 50 ppb. Outdoor sensing of aerosolized mixtures of (poly)cyclic aromatic hydrocarbons (PAHs), naphthalene and toluene was also realized. The reported platform can elucidate the characteristic vibrational fingerprints of each species within 10 s under the interference of a daylight background (Fig. 15d).

Min *et al.* also explored a SERS-active sensory array based on MIL-100(Fe) for ultrasensitive and multiplex detection of VOCs.[27] The LoD for toluene was 2.5 ppm on a solely MIL-100(Fe) substrate, and depositing gold nanoparticles over MIL-100 greatly amplified the signal with an enhancement factor of up to 10^{10}, which consequently reduced the LoD for toluene to 0.48 ppb. The high-SERS activity of MIL-100(Fe) can be accounted for by a charge transfer enhancement mechanism between the framework and the analytes, which was confirmed by the specific adsorption energy and DFT calculations. Specifically, the aromatic ligand and metal active sites are preferably combined by different molecules (*e.g.* toluene adsorption *via* π–π interaction and acetone *via* Fe–O coordination), providing sensor array properties for multiplex VOC detection. Finally, a MOF-integrated plasmonic surface-enhanced infrared adsorption platform was explored by Mu *et al.*, where ZIF-8 was coated on an Au antenna to realize on-chip sensing of greenhouse gases (CH_4 and CO_2).[195]

4. Conclusions and perspectives

This review summarizes recent progress on MOF-based colorimetric sensors with particular highlights on VOC sensing. The versatility of MOFs features their unique chemical and physical properties, drawing extensive research interest in them, especially as chemical sensing materials. The advancement of integrated circuits and miniaturization of electronic devices, combined with the development of MOF film fabrication, has recently allowed the preliminary laboratory demonstrations of practical VOC sensing application of MOFs.

Compared to research on MOF-based electronic sensors, research on MOF-based colorimetric sensors is still in the early stage. Chromism sensing exhibits a straightforward output with an often naked-eye observable colour change. The colorimetric responses highly rely on the design of MOF structures including modifying the coordination geometry of the metal sites in MOFs, using chromophoric ligands and encapsulating functional chromophores. Although many studies have demonstrated sensitive and selective sensing of VOCs using chromic MOFs, the delivered selectivity targets groups of VOCs and often lacks refined selectivity towards individual compounds as well as misses the examination of the materials under environmental conditions. The combination of multiple MOFs to create a sensor array can take advantage of the differentiated affinity of each MOF component and thus, an improved selectivity might be achieved. Besides, the shaping of colorimetric MOFs requires further attention, as it can also strongly influence the sensing performances. The reproducibility of nanoMOF-integrated sensing devices also needs critical recognition as it highly relies on the purity of MOFs, their activation status, and water-stability for consistent long-term performance. Luminescent sensing shares similar characteristics, where the intensity of luminescence is modified by the target analytes. The various choices of building blocks and diverse guest-recognition mechanisms have made luminescent MOFs rapidly evolve for sensing applications. The prominent challenge of luminescent MOFs is, similar to that of colorimetric MOFs, a lack of processability for practical implementations. Specifically, the construction of MOFs as thin films or membranes is starting, yet comprehensive evaluations of their performances including sensitivity, selectivity, response time, stability and recyclability still await further efforts. In addition, evaluating the luminescence change often requires specific instruments, which may pose additional obstacles to their practical applications. Overall, there is still a long journey ahead for chromism- and luminescent-based MOFs to achieve ultra-sensitive VOC sensing, especially for real-world sensing installation. Their limitation of sensitivity comes intrinsically from their sensing mechanisms, and thus colour-based sensors can hardly compete with other techniques such as SERS. Nonetheless, colour-based MOFs for VOC sensing possess their own advantages as they are easy to operate and interpret, not to mention the customizable selectivity provided by desired MOFs. Yet, one needs to note that the unique selective behaviour of MOFs is not a confirmation of outstanding sensing ability. It is also worth

Open Access Article. Published on 05 lokakuuta 2022. Downloaded on 8.6.2026 20.57.17.
This article is licensed under a Creative Commons Attribution-NonCommercial 3.0 Unported Licence.

investigating and examining promising materials under different circumstances. To summarize, despite the advantage of naked-eye observation, limited studies examined chromic and luminescent MOFs in the presence of VOC vapors and sensing performance was often not systematically investigated. The reported LoD of some chromic or luminescent MOFs falls within the ppm levels and can be varied greatly depending on the chosen MOFs. It is worth mentioning that their sensitivity is sometimes limited by the sensing mechanisms, especially for the ones relying on ligand-to-metal transfer, which are often less sensitive than the organic-based system. Furthermore, considering that the shaping processes are not often developed with these compounds, considerable efforts are still required in order to use these types of MOFs in real devices.

Other optical sensors are based on the change of the optical index induced by the absorbance of analytes on the MOF sensing layer. For such purposes, multiple techniques have integrated MOFs in the form of thin films or photonic crystals into sensing devices. They present great potential in VOC vapour sensing with sensitivity from the ppb to the ppm level. In particular, Fabry–Perot interferometers can efficiently transduce adsorption-induced refractive index change, with sensing performances including sensitivity, selectivity and response time that are highly associated with the sorption features of integrated MOF layers. MOF sorption ability not only depends on their microstructure and intrinsic physico-chemical properties but is also related to the attributes of MOF-film engineering. Reducing the thickness of MOF films can accelerate the mass-transport process of analytes, but at the same time, can damage the optical properties of the sensor by diminishing the magnitude of the RI, leading to undermined performance. Furthermore, the orientation of MOF particles can also impact the optical properties of the film, as highly oriented films can enhance both the selectivity[112] and signal intensity for potential colorimetric sensing. Another possible strategy to optimize the signal transduction is the hybridization of MOFs with oxide nanoparticles. One way is to integrate MOF photonic crystals into Bragg stacks with contrasting oxide NPs, which requires size and morphology control during MOF synthesis. The other approach is by encapsulating oxide NPs into MOF films; however, obtaining a uniform and homogenous distribution of NPs is still challenging.

Optical fibres based on RI changes can also encode sensing events into spectra. They are known for their immunity to electromagnetic interference and are generally light weight with small probe heads and high flexibility, which allows highly sensitive and multiplex detection in remote or harsh environments. The MOF coatings in optical fibres act as concentrators to boost the sensitivity (LoD under 10 ppm) and also potentially as sieving layers for enhanced selectivity. However, it is, like the aforementioned others, a technique under preliminary investigation, as only ZIF-8 was coated on the fibres and ethanol was the only tested vapor. Thus, the selectivity of this method must still be explored. The mechanical properties of the MOF coating are key factors for the practical integration of MOFs into optical fibres. *In situ* growth of MOF films is widely adopted for optical fibre coating. Despite the convenience of this method, it is challenging to precisely control the morphology and defects of the film, as well as not being easily scalable. Besides, mismatching MOFs with weakly adhered optical fibres can cause damage to the MOF coating (*e.g.* cracks and shedding), thus hindering the performance of the sensor. MOF-polymer-based mixed-matrix membranes might be an alternative solution to tackle such drawbacks, yet a systematic investigation is still required.

SERS is recognized as a highly sensitive and selective technique for quantitative detection of chemicals at trace levels. MOFs have been identified as Raman active substrates and, with appropriate choices of candidates, their enhancement factor can be competitive with classic SERS substrates including noble metal NPs. These MOF-based SERS systems have been actively applied in vapour-phase sensing with promising processes recently. Configuration of core–shell structures between MOFs and plasmonic noble metal NPs is also a popular strategy to improve sensing performances *via* enhanced substrate-analyte affinity or molecular trapping.

As multiple sensing techniques are involved in this review, it is also important to compare them for their performance and potential in practical applications. The detection and monitoring of VOCs in the real world require sufficient sensitivity of sensors considering the toxicity and exposure limits of VOCs, especially carcinogenic ones including benzene, formaldehyde, toluene, *etc.* For example, the exposure limit of formaldehyde regulated by the EU is 300 ppb for 8 h of average exposure and 600 ppb for short term exposure (data from the GESTIS database). The LoD of MOF-incorporated colorimetric and luminescent sensing is grouped around the ppm level, as it is mostly preliminary research. Micro-ring resonators, SPP resonance, and SERS can handle ppb-level detection. However, micro-ring resonators with MOF coating and SPP resonance are currently at the proof-of-concept level. Their performance under practical conditions including interfering gases/vapors and humidity needs further examination. At the current stage, SERS can be considered as the platform closest to the actual application for its refined LoD (lowest report value of 0.48 ppb) and fast response time (several seconds). The cost of MOFs is a generally concerning topic when speaking about their real application due to harsh synthetic conditions limiting the production scale and their price. Optimizing MOF synthesis and large-scale production are the two contributing factors that can benefit MOFs' practical use.

The key challenge for MOF-based SERS, as well as for other MOF-integrated proof-of-concept techniques, is to expand the spectrum of MOF candidates. The majority of research on sensing applications employed limited benchmark MOFs such as ZIF-8 or HKUST-1, due to their well-developed facile synthesis and diverse shaping approaches. However, they have drawbacks including poor chemical stability (HKUST-1), insufficient water stability and the narrow pore sizes of ZIF-8(4 Å) that limit their potential for practical usage, especially in large-molecule sensing. Besides, difficulty in functionalization further hinders them by restricting tailorability for desired analytes. Conventional one-pot MOF synthesis generally acquires harsh conditions (*e.g.* high pressure and temperature), especially for

© 2022 The Author(s). Published by the Royal Society of Chemistry

Open Access Article. Published on 05 lokakuuta 2022. Downloaded on 8.6.2026 20.57.17.
This article is licensed under a Creative Commons Attribution-NonCommercial 3.0 Unported Licence.

water-stable high-valence MOFs, which makes it complicated to further incorporate with nanoparticles. Thus, developments in the mild-condition synthesis of MOFs are expected to promote a further diverse application, where the potential of MOFs can be fully explored.

Author contributions

Y. S. wrote the manuscript. A. T. and C. S. revised and supervised the manuscript.

Conflicts of interest

There are no conflicts of interest to declare.

Acknowledgements

YS thanks the UptoParis European Union's Horizon 2020 research and innovation program under the Marie Skłodowska-Curie grant agreement No. 754387.

References

1 S. Joshi, The Sick Building Syndrome, *Indian Journal of Occupational and Environmental Medicine*, 2008, **12**(2), 61, DOI: 10.4103/0019-5278.43262.

2 D. A. Sarigiannis, S. P. Karakitsios, A. Gotti, I. L. Liakos and A. Katsoyiannis, Exposure to Major Volatile Organic Compounds and Carbonyls in European Indoor Environments and Associated Health Risk, *Environ. Int.*, 2011, **37**(4), 743–765, DOI: 10.1016/j.envint.2011.01.005.

3 M. R. Ras, F. Borrull and R. M. Marcé, Sampling and Preconcentration Techniques for Determination of Volatile Organic Compounds in Air Samples, *TrAC, Trends Anal. Chem.*, 2009, **28**(3), 347–361, DOI: 10.1016/j.trac.2008.10.009.

4 Y. Zhang, J. Zhao, T. Du, Z. Zhu, J. Zhang and Q. Liu, A Gas Sensor Array for the Simultaneous Detection of Multiple VOCs, *Sci. Rep.*, 2017, **7**(1), 1–8, DOI: 10.1038/s41598-017-02150-z.

5 J. Park and H. Tabata, Gas Sensor Array Using a Hybrid Structure Based on Zeolite and Oxide Semiconductors for Multiple Bio-Gas Detection, *ACS Omega*, 2021, **6**(33), 21284–21293, DOI: 10.1021/ACSOMEGA.1C01435.

6 O. M. Yaghi, M. O'Keeffe, N. W. Ockwig, H. K. Chae, M. Eddaoudi and J. Kim, Reticular Synthesis and the Design of New Materials, *Nature*, 2003, **423**(6941), 705–714, DOI: 10.1038/NATURE01650.

7 A. J. Howarth, Y. Liu, P. Li, Z. Li, T. C. Wang, J. T. Hupp and O. K. Farha, Chemical, Thermal and Mechanical Stabilities of Metal-Organic Frameworks, *Nat. Rev. Mater.*, 2016, **1**(15018), 1–15, DOI: 10.1038/natrevmats.2015.18.

8 F. Bigdeli, C. T. Lollar, A. Morsali and H. C. Zhou, Switching in Metal–Organic Frameworks, *Angew. Chem., Int. Ed.*, 2020, **59**(12), 4652–4669, DOI: 10.1002/ANIE.201900666.

9 Z. Niu, X. Cui, T. Pham, G. Verma, P. C. Lan, C. Shan, H. Xing, K. A. Forrest, S. Suepaul, B. Space, A. Nafady, A. M. Al-Enizi and S. Ma, A MOF-Based Ultra-Strong Acetylene Nano-Trap for Highly Efficient C_2H_2/CO_2 Separation, *Angew. Chem., Int. Ed.*, 2021, **60**(10), 5283–5288, DOI: 10.1002/anie.202016225.

10 H. Fan, M. Peng, I. Strauss, A. Mundstock, H. Meng and J. Caro, MOF-in-COF Molecular Sieving Membrane for Selective Hydrogen Separation, *Nat. Commun.*, 2021, **12**(1), 1–10, DOI: 10.1038/s41467-020-20298-7.

11 Y. Li, H. Liu, H. Wang, J. Qiu and X. Zhang, GO-Guided Direct Growth of Highly Oriented Metal–Organic Framework Nanosheet Membranes for H_2/CO_2 Separation, *Chem. Sci.*, 2018, **9**(17), 4132–4141, DOI: 10.1039/C7SC04815G.

12 D. E. Jaramillo, A. Jaffe, B. E. R. Snyder, A. Smith, E. Taw, R. C. Rohde, M. N. Dods, W. DeSnoo, K. R. Meihaus, T. D. Harris, J. B. Neaton and J. R. Long, Metal–Organic Frameworks as O_2-Selective Adsorbents for Air Separations, *Chem. Sci.*, 2022, **13**(35), 10216–10237, DOI: 10.1039/D2SC03577D.

13 M. Bonneau, C. Lavenn, P. Ginet, K. I. Otake and S. Kitagawa, Upscale Synthesis of a Binary Pillared Layered MOF for Hydrocarbon Gas Storage and Separation, *Green Chem.*, 2020, **22**(3), 718–724, DOI: 10.1039/C9GC03561C.

14 O. K. Farha, A. Ö. Yazaydin, I. Eryazici, C. D. Malliakas, B. G. Hauser, M. G. Kanatzidis, S. T. Nguyen, R. Q. Snurr and J. T. Hupp, De Novo Synthesis of a Metal–Organic Framework Material Featuring Ultrahigh Surface Area and Gas Storage Capacities, *Nat. Chem.*, 2010, **2**(11), 944–948, DOI: 10.1038/nchem.834.

15 T. Wang, L. Gao, J. Hou, S. J. A. Herou, J. T. Griffiths, W. Li, J. Dong, S. Gao, M. M. Titirici, R. V. Kumar, A. K. Cheetham, X. Bao, Q. Fu and S. K. Smoukov, Rational Approach to Guest Confinement inside MOF Cavities for Low-Temperature Catalysis, *Nat. Commun.*, 2019, **10**(1), 1–9, DOI: 10.1038/s41467-019-08972-x.

16 S. Dai, K. P. Ngoc, L. Grimaud, S. Zhang, A. Tissot and C. Serre, Impact of Capping Agent Removal from Au NPs@MOF Core–Shell Nanoparticle Heterogeneous Catalysts, *J. Mater. Chem. A*, 2022, **10**(6), 3201–3205, DOI: 10.1039/D1TA09108E.

17 N. Heidary, D. Chartrand, A. Guiet and N. Kornienko, Rational Incorporation of Defects within Metal–Organic Frameworks Generates Highly Active Electrocatalytic Sites, *Chem. Sci.*, 2021, **12**(21), 7324–7333, DOI: 10.1039/D1SC00573A.

18 K. Suresh and A. J. Matzger, Enhanced Drug Delivery by Dissolution of Amorphous Drug Encapsulated in a Water Unstable Metal–Organic Framework (MOF), *Angew. Chem., Int. Ed.*, 2019, **58**(47), 16790–16794, DOI: 10.1002/ANIE.201907652.

19 E. Gkaniatsou, C. Sicard, R. Ricoux, L. Benahmed, F. Bourdreux, Q. Zhang, C. Serre, J.-P. Mahy and N. Steunou, Enzyme Encapsulation in Mesoporous Metal–Organic Frameworks for Selective Biodegradation of Harmful Dye Molecules, *Angew. Chem., Int. Ed.*, 2018, **57**(49), 16141–16146, DOI: 10.1002/anie.201811327.

Open Access Article. Published on 05 lokakuuta 2022. Downloaded on 8.6.2026 20.57.17.
This article is licensed under a Creative Commons Attribution-NonCommercial 3.0 Unported Licence.

20 R. V. Pinto, S. Wang, S. R. Tavares, J. Pires, F. Antunes, A. Vimont, G. Clet, M. Daturi, G. Maurin, C. Serre and M. L. Pinto, Tuning Cellular Biological Functions through the Controlled Release of NO from a Porous Ti-MOF, *Angew. Chem., Int. Ed.*, 2020, **59**(13), 5135–5143, DOI: **10.1002/ANIE.201913135**.

21 H. Yuan, N. Li, W. Fan, H. Cai, D. Zhao, H. Yuan, W. Fan, D. Zhao, N. Li and H. Cai, Metal-Organic Framework Based Gas Sensors, *Adv. Sci.*, 2021, 2104374, DOI: **10.1002/ADVS.202104374**.

22 Z. Meng, R. M. Stolz, L. Mendecki and K. A. Mirica, Electrically-Transduced Chemical Sensors Based on Two-Dimensional Nanomaterials, *Chem. Rev.*, 2019, **119**(1), 478–598, DOI: **10.1021/ACS.CHEMREV.8B00311**.

23 L.-T. Zhang, Y. Zhou and S.-T. Han, The Role of Metal–Organic Frameworks in Electronic Sensors, *Angew. Chem., Int. Ed.*, 2021, **60**(28), 15192–15212, DOI: **10.1002/ANIE.202006402**.

24 H.-Y. Li, S.-N. Zhao, S.-Q. Zang and J. Li, Functional Metal-Organic Frameworks as Effective Sensors of Gases and Volatile Compounds, *Chem. Soc. Rev.*, 2020, **49**, 6364, DOI: **10.1039/c9cs00778d**.

25 J. D. Humby, O. Benson, G. L. Smith, S. P. Argent, I. Da Silva, Y. Cheng, S. Rudić, P. Manuel, M. D. Frogley, G. Cinque, L. K. Saunders, I. J. Vitórica-Yrezábal, G. F. S. Whitehead, T. L. Easun, W. Lewis, A. J. Blake, A. J. Ramirez-Cuesta, S. Yang and M. Schröder, Host–Guest Selectivity in a Series of Isoreticular Metal–Organic Frameworks: Observation of Acetylene-to-Alkyne and Carbon Dioxide-to-Amide Interactions, *Chem. Sci.*, 2019, **10**(4), 1098–1106, DOI: **10.1039/C8SC03622E**.

26 Z. Ma, T. Yuan, Y. Fan, L. Wang, Z. Duan, W. Du, D. Zhang and J. Xu, A Benzene Vapor Sensor Based on a Metal-Organic Framework-Modified Quartz Crystal Microbalance, *Sens. Actuators, B*, 2020, **311**, 127365, DOI: **10.1016/j.snb.2019.127365**.

27 J.-H. Fu, Z. Zhong, D. Xie, Y.-J. Guo, D.-X. Kong, Z.-X. Zhao, Z.-X. Zhao and M. Li, SERS-Active MIL-100(Fe) Sensory Array for Ultrasensitive and Multiplex Detection of VOCs, *Angew. Chem., Int. Ed.*, 2020, **59**(46), 20489–20498, DOI: **10.1002/ANIE.202002720**.

28 M. R. Tchalala, P. M. Bhatt, K. N. Chappanda, S. R. Tavares, K. Adil, Y. Belmabkhout, A. Shkurenko, A. Cadiau, N. Heymans, G. De Weireld, G. Maurin, K. N. Salama and M. Eddaoudi, Fluorinated MOF Platform for Selective Removal and Sensing of SO_2 from Flue Gas and Air, *Nat. Commun.*, 2019, **10**(1), 1328, DOI: **10.1038/s41467-019-09157-2**.

29 J. Tao, X. Wang, T. Sun, H. Cai, Y. Wang, T. Lin, D. Fu, L. Lee, Y. Ting, Y. Gu and D. Zhao, Hybrid Photonic Cavity with Metal-Organic Framework Coatings for the Ultra-Sensitive Detection of Volatile Organic Compounds with High Immunity to Humidity, *Sci. Rep.*, 2017, **7**, 41640, DOI: **10.1038/srep41640**.

30 H. H.-M. Yeung, G. Yoshikawa, K. Minami and K. Shiba, Strain-Based Chemical Sensing Using Metal–Organic Framework Nanoparticles, *J. Mater. Chem. A*, 2020, **8**(35), 18007–18014, DOI: **10.1039/D0TA07248F**.

31 P. Mü, F. M. Wisser, P. Freund, V. Bon, I. Senkovska and S. Kaskel, Optical Sensors Using Solvatochromic Metal–Organic Frameworks, *Inorg. Chem.*, 2017, **56**(22), 14164–14169, DOI: **10.1021/acs.inorgchem.7b02241**.

32 A. Tissot, X. Kesse, S. Giannopoulou, I. Stenger, L. Binet, E. Rivière and C. Serre, A Spin Crossover Porous Hybrid Architecture for Potential Sensing Applications, *Chem. Commun.*, 2019, **55**(2), 194–197, DOI: **10.1039/C8CC07573E**.

33 P. Qin, S. Okur, C. Li, A. Chandresh, D. Mutruc, S. Hecht and L. Heinke, A Photoprogrammable Electronic Nose with Switchable Selectivity for VOCs Using MOF Films, *Chem. Sci.*, 2021, **12**(47), 15700–15709, DOI: **10.1039/D1SC05249G**.

34 M. Eddaoudi, J. Kim, N. Rosi, D. Vodak, J. Wachter, M. O'Keeffe and O. M. Yaghi, Systematic Design of Pore Size and Functionality in Isoreticular MOFs and Their Application in Methane Storage, *Science*, 2002, **295**(5554), 469–472, DOI: **10.1126/SCIENCE.1067208**.

35 H. Deng, C. J. Doonan, H. Furukawa, R. B. Ferreira, J. Towne, C. B. Knobler, B. Wang and O. M. Yaghi, Multiple Functional Groups of Varying Ratios in Metal-Organic Frameworks, *Science*, 2010, **327**(5967), 846–850, DOI: **10.1126/SCIENCE.1181761**.

36 A. W. Thornton, R. Babarao, A. Jain, F. Trousselet and F. X. Coudert, Defects in Metal–Organic Frameworks: A Compromise between Adsorption and Stability?, *Dalton Trans.*, 2016, **45**(10), 4352–4359, DOI: **10.1039/C5DT04330A**.

37 H. Yuan, J. Tao, N. Li, A. Karmakar, C. Tang, H. Cai, S. J. Pennycook, N. Singh and D. Zhao, On-Chip Tailorability of Capacitive Gas Sensors Integrated with Metal–Organic Framework Films, *Angew. Chem., Int. Ed.*, 2019, **58**(40), 14089–14094, DOI: **10.1002/anie.201906222**.

38 C. T. Lee and M. W. Shin, Solvothermal Growth of Mg-MOF-74 Films on Carboxylic Functionalized Silicon Substrate Using Acrylic Acid, *Surf. Interfaces*, 2021, **22**, 100845, DOI: **10.1016/J.SURFIN.2020.100845**.

39 X. Zhang, K. Wan, P. Subramanian, M. Xu, J. Luo and J. Fransaer, Electrochemical Deposition of Metal–Organic Framework Films and Their Applications, *J. Mater. Chem. A*, 2020, **8**(16), 7569–7587, DOI: **10.1039/D0TA00406E**.

40 D. Jiang, A. D. Burrows, Y. Xiong and K. J. Edler, Facile Synthesis of Crack-Free Metal–Organic Framework Films on Alumina by a Dip-Coating Route in the Presence of Polyethylenimine, *J. Mater. Chem. A*, 2013, **1**(18), 5497–5500, DOI: **10.1039/C3TA10766C**.

41 P. Horcajada, C. Serre, D. Grosso, C. Boissiè, S. Perruchas, C. Sanchez, G. Férey, C. Sanchez, D. Grosso, C. Boissiè, G. Férey, P. Horcajada, C. Serre and S. Perruchas, Colloidal Route for Preparing Optical Thin Films of Nanoporous Metal–Organic Frameworks, *Adv. Mater.*, 2009, **21**(19), 1931–1935, DOI: **10.1002/ADMA.200801851**.

42 E. Ahvenniemi and M. Karppinen, Atomic/Molecular Layer Deposition: A Direct Gas-Phase Route to Crystalline Metal–Organic Framework Thin Films, *Chem. Commun.*, 2016, **52**(6), 1139–1142, DOI: **10.1039/C5CC08538A**.

© 2022 The Author(s). Published by the Royal Society of Chemistry

Open Access Article. Published on 05 lokakuuta 2022. Downloaded on 8.6.2026 20.57.17.
This article is licensed under a Creative Commons Attribution-NonCommercial 3.0 Unported Licence.

43 L. D. Salmi, M. J. Heikkilä, E. Puukilainen, T. Sajavaara, D. Grosso and M. Ritala, Studies on Atomic Layer Deposition of MOF-5 Thin Films, *Microporous Mesoporous Mater.*, 2013, **182**, 147–154, DOI: 10.1016/J.MICROMESO.2013.08.024.

44 K. B. Lausund and O. Nilsen, All-Gas-Phase Synthesis of UiO-66 through Modulated Atomic Layer Deposition, *Nat. Commun.*, 2016, **7**(1), 1–9, DOI: 10.1038/ncomms13578.

45 X.-J. Yu, Y.-M. Xian, C. Wang, H.-L. Mao, M. Kind, T. Abu-Husein, Z. Chen, S.-B. Zhu, B. Ren, A. Terfort and J.-L. Zhuang, Liquid-Phase Epitaxial Growth of Highly Oriented and Multivariate Surface-Attached Metal–Organic Frameworks, *J. Am. Chem. Soc.*, 2019, **141**, 21, DOI: 10.1021/jacs.9b08169.

46 A. Summerfield, I. Cebula, M. Schrö Der and P. H. Beton, Nucleation and Early Stages of Layer-by-Layer Growth of Metal Organic Frameworks on Surfaces, *J. Phys. Chem. C*, 2015, **119**, 2022, DOI: 10.1021/acs.jpcc.5b07133.

47 J. Liu, B. Lukose, O. Shekhah, H. K. Arslan, P. Weidler, H. Gliemann, S. Bräse, S. Grosjean, A. Godt, X. Feng, K. Müllen, I. B. Magdau, T. Heine and C. Wöll, A Novel Series of Isoreticular Metal Organic Frameworks: Realizing Metastable Structures by Liquid Phase Epitaxy, *Sci. Rep.*, 2012, **2**(1), 1–5, DOI: 10.1038/srep00921.

48 A. Bétard and R. A. Fischer, Metal-Organic Framework Thin Films: From Fundamentals to Applications, *Chem. Rev.*, 2012, **112**(2), 1055–1083, DOI: 10.1021/cr200167v.

49 P. Falcaro, D. Buso, A. J. Hill, C. M. Doherty, P. Falcaro, D. Buso, A. J. Hill and C. M. Doherty, Patterning Techniques for Metal Organic Frameworks, *Adv. Mater.*, 2012, **24**(24), 3153–3168, DOI: 10.1002/ADMA.201200485.

50 P. Falcaro, R. Ricco, C. M. Doherty, K. Liang, A. J. Hill and M. J. Styles, MOF Positioning Technology and Device Fabrication, *Chem. Soc. Rev.*, 2014, **43**(16), 5513–5560, DOI: 10.1039/C4CS00089G.

51 P. Falcaro, R. Ricco, C. M. Doherty, K. Liang, A. J. Hill and M. J. Styles, MOF Positioning Technology and Device Fabrication, *Chem. Soc. Rev.*, 2014, **43**(16), 5513–5560, DOI: 10.1039/C4CS00089G.

52 R. Dong, T. Zhang and X. Feng, Interface-Assisted Synthesis of 2D Materials: Trend and Challenges, *Chem. Rev.*, 2018, **118**(13), 6189–6325, DOI: 10.1021/ACS.CHEMREV.8B00056.

53 I. Stassen, N. Burtch, A. Talin, P. Falcaro, M. Allendorf and R. Ameloot, An Updated Roadmap for the Integration of Metal–Organic Frameworks with Electronic Devices and Chemical Sensors, *Chem. Soc. Rev.*, 2017, **46**(11), 3185–3241, DOI: 10.1039/C7CS00122C.

54 G. Chakraborty, I. H. Park, R. Medishetty and J. J. Vittal, Two-Dimensional Metal-Organic Framework Materials: Synthesis, Structures, Properties and Applications, *Chem. Rev.*, 2021, **121**(7), 3751–3891, DOI: 10.1021/ACS.CHEMREV.0C01049.

55 M. D. Allendorf, R. Dong, X. Feng, S. Kaskel, D. Matoga and V. Stavila, Electronic Devices Using Open Framework Materials, *Chem. Rev.*, 2020, 8581–8640, DOI: 10.1021/acs.chemrev.0c00033.

56 J. Ren and T. C. Jen, Atomic Layer Deposition (ALD) Assisting the Visibility of Metal-Organic Frameworks (MOFs) Technologies, *Coord. Chem. Rev.*, 2021, **430**, 213734, DOI: 10.1016/J.CCR.2020.213734.

57 C. Sanchez, K. J. Shea, S. Kitagawa, O. Shekhah, J. Liu, R. A. Fischer and C. Woïl, Hybrid Materials Themed Issue MOF Thin Films: Existing and Future Applications, *Chem. Soc. Rev.*, 2011, **4**, 1081–1106, DOI: 10.1039/c0cs00147c.

58 Z. Wang, L. Liu, Z. Li, N. Goyal, T. Du, J. He and G. K. Li, Shaping of Metal-Organic Frameworks: A Review, *Energy Fuels*, 2022, **36**(6), 2927–2944, DOI: 10.1021/acs.energyfuels.1c03426.

59 D. Zacher, A. Baunemann, S. Hermes and R. A. Fischer, Deposition of Microcrystalline $[Cu_3(Btc)_2]$ and $[Zn_2(Bdc)_2(Dabco)]$ at Alumina and Silica Surfaces Modified with Patterned Self Assembled Organic Monolayers: Evidence of Surface Selective and Oriented Growth, *J. Mater. Chem.*, 2007, **17**(27), 2785–2792, DOI: 10.1039/b703098c.

60 J. Liu, F. Sun, F. Zhang, Z. Wang, R. Zhang, C. Wang and S. Qiu, In Situ Growth of Continuous Thin Metal–Organic Framework Film for Capacitive Humidity Sensing, *J. Mater. Chem.*, 2011, **21**(11), 3775–3778, DOI: 10.1039/C0JM03123B.

61 H. Ji, S. Hwang, K. Kim, C. Kim and N. C. Jeong, Direct In Situ Conversion of Metals into Metal-Organic Frameworks: A Strategy for the Rapid Growth of MOF Films on Metal Substrates, *ACS Appl. Mater. Interfaces*, 2016, **8**(47), 32414–32420, DOI: 10.1021/ACSAMI.6B12755.

62 A. Centrone, Y. Yang, S. Speakman, L. Bromberg, G. C. Rutledge and T. A. Hatton, Growth of Metal-Organic Frameworks on Polymer Surfaces, *J. Am. Chem. Soc.*, 2010, **132**(44), 15687–15691, DOI: 10.1021/JA106381X.

63 P. K. Verma, L. Huelsenbeck, A. W. Nichols, T. Islamoglu, H. Heinrich, C. W. Machan and G. Giri, Controlling Polymorphism and Orientation of NU-901/NU-1000 Metal-Organic Framework Thin Films, *Chem. Mater.*, 2020, **32**(24), 10556–10565, DOI: 10.1021/ACS.CHEMMATER.0C03539.

64 H. Yuan, W. Fu, N. Soulmi, C. Serre, N. Steunou, M. Rosso and C. Henry de Villeneuve, Growth of Fe-BDC Metal-Organic Frameworks onto Functionalized Si(111) Surfaces, *Chem.–Asian J.*, 2022, **17**(13), e202200129, DOI: 10.1002/ASIA.202200129.

65 A. Ulman, Formation and Structure of Self-Assembled Monolayers, *Chem. Rev.*, 1996, **96**(4), 1533–1554, DOI: 10.1021/CR9502357.

66 H. Yuan, *Growth of Metal Organic Frameworks (MOFs) Layers on Functionalized Surfaces*, 2019.

67 C. Carbonell, I. Imaz and D. Maspoch, Single-Crystal Metal-Organic Framework Arrays, *J. Am. Chem. Soc.*, 2011, **133**(7), 2144–2147, DOI: 10.1021/JA2002428.

68 S. Hermes, F. Schröder, R. Chelmowski, C. Wöll and R. A. Fischer, Selective Nucleation and Growth of Metal-Organic Open Framework Thin Films on Patterned $COOH/CF_3$-Terminated Self-Assembled Monolayers on

Open Access Article. Published on 05 lokakuuta 2022. Downloaded on 8.6.2026 20.57.17.
This article is licensed under a Creative Commons Attribution-NonCommercial 3.0 Unported Licence.

Au(111), *J. Am. Chem. Soc.*, 2005, **127**(40), 13744–13745, DOI: 10.1021/JA053523L.

69 H. Yang and H. Fei, A Generic and Facile Strategy to Fabricate Metal–Organic Framework Films on TiO_2 Substrates for Photocatalysis, *Dalton Trans.*, 2017, **46**(9), 2751–2755, DOI: 10.1039/C7DT00082K.

70 C. W. Kung, T. H. Chang, L. Y. Chou, J. T. Hupp, O. K. Farha and K. C. Ho, Post Metalation of Solvothermally Grown Electroactive Porphyrin Metal–Organic Framework Thin Films, *Chem. Commun.*, 2015, **51**(12), 2414–2417, DOI: 10.1039/C4CC09272D.

71 C. Scherb, A. Schödel and T. Bein, Directing the Structure of Metal-Organic Frameworks by Oriented Surface Growth on an Organic Monolayer, *Angew. Chem., Int. Ed.*, 2008, **47**(31), 5777–5779, DOI: 10.1002/ANIE.200704034.

72 A. Rosenhahn, S. Schilp, H. Jürgen Kreuzer, M. Grunze, D. A. Egger, F. Rissner, G. M. Rangger, O. T. Hofmann, L. Wittwer, G. Heimel, E. Zojer, L. Wang, Z. Ma, Q. Li, Z. Shuai, P. Chem, C. Zhang, J. Grandner, R. Liu, S. Bok Lee, B. W. Eichhorn, J. Duay, T. Lane, R. Baumann, M. Schranz, N. Hampp, P. Chem Chem, L. B. Thompson, N. H. Mack, R. G. Nuzzo, S. Kuhn, B. Baisch, U. Jung, T. Johannsen, J. Kubitschke, R. Herges, O. Magnussen, P. Mahanandia, J. J. Schneider, M. Khaneft, B. Stühn, T. P. Peixoto, B. Drossel, H. Liang, Z. Li, J. Yang, N. Bonnet, G. Hähner, R. Dabirian, X. Feng, L. Ortolani, A. Liscio, V. Morandi, K. Müllen, P. Samorì, V. Palermo, P. Duan and M. Liu, Oriented Growth of the Functionalized Metal–Organic Framework CAU-1 on –OH- and –COOH-Terminated Self-Assembled Monolayers, *Phys. Chem. Chem. Phys.*, 2010, **12**(17), 4515–4520, DOI: 10.1039/B924657F.

73 E. Biemmi, C. Scherb and T. Bein, Oriented Growth of the Metal Organic Framework $Cu_3(BTC)\cdot 2(H_2O)_3\cdot xH_2O$ Tunable with Functionalized Self-Assembled Monolayers, *J. Am. Chem. Soc.*, 2007, **129**(26), 8054–8055, DOI: 10.1021/JA0701208.

74 J. Liu and C. Wöll, Surface-Supported Metal–Organic Framework Thin Films: Fabrication Methods, Applications, and Challenges, *Chem. Soc. Rev.*, 2017, **46**(19), 5730–5770, DOI: 10.1039/C7CS00315C.

75 S. Li, W. Shi, G. Lu, S. Li, S. C. J. Loo and F. Huo, Unconventional Nucleation and Oriented Growth of ZIF-8 Crystals on Non-Polar Surface, *Adv. Mater.*, 2012, **24**(44), 5954–5958, DOI: 10.1002/ADMA.201201996.

76 T. Ladnorg, A. Welle, S. Heißler, C. Wöll and H. Gliemann, Site-Selective Growth of Surface-Anchored Metal-Organic Frameworks on Self-Assembled Monolayer Patterns Prepared by AFM Nanografting, *Beilstein J. Nanotechnol.*, 2013, **4**(1), 638–648, DOI: 10.3762/BJNANO.4.71.

77 H. K. Arslan, O. Shekhah, J. Wohlgemuth, M. Franzreb, R. A. Fischer and C. Wöll, High-throughput Fabrication of Uniform and Homogenous MOF Coatings, *Adv. Funct. Mater.*, 2011, **21**(22), 4228–4231, DOI: 10.1002/ADFM.201101592.

78 R. Makiura, S. Motoyama, Y. Umemura, H. Yamanaka, O. Sakata and H. Kitagawa, Surface Nano-Architecture of a Metal–Organic Framework, *Nat. Mater.*, 2010, **9**(7), 565–571, DOI: 10.1038/nmat2769.

79 J. L. Zhuang, A. Terfort and C. Wöll, Formation of Oriented and Patterned Films of Metal–Organic Frameworks by Liquid Phase Epitaxy: A Review, *Coord. Chem. Rev.*, 2016, **307**, 391–424, DOI: 10.1016/J.CCR.2015.09.013.

80 P. Falcaro, K. Okada, T. Hara, K. Ikigaki, Y. Tokudome, A. W. Thornton, A. J. Hill, T. Williams, C. Doonan and M. Takahashi, Centimetre-Scale Micropore Alignment in Oriented Polycrystalline Metal-Organic Framework Films via Heteroepitaxial Growth, *Nat. Mater.*, 2017, **16**(3), 342–348, DOI: 10.1038/NMAT4815.

81 I. Stassen, M. Styles, G. Grenci, H. Van Gorp, W. Vanderlinden, S. De Feyter, P. Falcaro, D. De Vos, P. Vereecken and R. Ameloot, Chemical Vapour Deposition of Zeolitic Imidazolate Framework Thin Films, *Nat. Mater.*, 2015, **15**(3), 304–310, DOI: 10.1038/nmat4509.

82 P. Su, M. Tu, R. Ameloot and W. Li, Vapor-Phase Processing of Metal-Organic Frameworks, *Acc. Chem. Res.*, 2022, **55**(2), 186–196, DOI: 10.1021/acs.accounts.1c00600.

83 Z. Zhang, Y. Zhao, Z. Zhao, G. Huang and Y. Mei, *Atomic Layer Deposition-Derived Nanomaterials: Oxides, Transition Metal Dichalcogenides, and Metal–Organic Frameworks*, 2020, DOI: DOI: 10.1021/acs.chemmater.9b04414.

84 A. Tanskanen and M. Karppinen, Iron-Terephthalate Coordination Network Thin Films through In-Situ Atomic/Molecular Layer Deposition, *Sci. Rep.*, 2018, **8**(1), 1–8, DOI: 10.1038/s41598-018-27124-7.

85 E. Virmani, J. M. Rotter, A. Mähringer, T. Von Zons, A. Godt, T. Bein, S. Wuttke and D. D. Medina, On-Surface Synthesis of Highly Oriented Thin Metal-Organic Framework Films through Vapor-Assisted Conversion, *J. Am. Chem. Soc.*, 2018, **140**(14), 4812–4819, DOI: 10.1021/jacs.7b08174.

86 C. Crivello, S. Sevim, O. Graniel, C. Franco, S. Pané, J. Puigmartí-Luis and D. Muñoz-Rojas, Advanced Technologies for the Fabrication of MOF Thin Films, *Mater. Horiz.*, 2021, **8**, 168–178, DOI: 10.1039/D0MH00898B.

87 S. Jia, D. Ji, L. Wang, X. Qin and S. Ramakrishna, Metal–Organic Framework Membranes: Advances, Fabrication, and Applications, *Small Struct.*, 2022, **3**(4), 2100222, DOI: 10.1002/SSTR.202100222.

88 J. Benito, S. Sorribas, I. Lucas, J. Coronas and I. Gascon, Langmuir-Blodgett Films of the Metal-Organic Framework MIL-101(Cr): Preparation, Characterization, and CO_2 Adsorption Study Using a QCM-Based Setup, *ACS Appl. Mater. Interfaces*, 2016, **8**(25), 16486–16492, DOI: 10.1021/ACSAMI.6B04272.

89 M. A. Andrés, C. Sicard, C. Serre, O. Roubeau and I. Gascón, Ultrathin Hydrophobic Films Based on the Metal Organic Framework UiO-66-COOH(Zr), *Beilstein J. Nanotechnol.*, 2019, **10**, 654–665, DOI: 10.3762/bjnano.10.65.

90 M. A. Andrés, M. Benzaqui, C. Serre, N. Steunou and I. Gascón, Fabrication of Ultrathin MIL-96(Al) Films and Study of CO_2 Adsorption/Desorption Processes Using Quartz Crystal Microbalance, *J. Colloid Interface Sci.*, 2018, **519**, 88–96, DOI: 10.1016/J.JCIS.2018.02.058.

© 2022 The Author(s). Published by the Royal Society of Chemistry

Open Access Article. Published on 05 lokakuuta 2022. Downloaded on 8.6.2026 20.57.17.
This article is licensed under a Creative Commons Attribution-NonCommercial 3.0 Unported Licence.

91 S. Rauf, M. A. Andrés, O. Roubeau, I. Gascón, C. Serre, M. Eddaoudi and K. N. Salama, Coating of Conducting and Insulating Threads with Porous MOF Particles through Langmuir-Blodgett Technique, *Nanomaterials*, 2021, **11**(1), 160, DOI: 10.3390/NANO11010160.

92 M. A. Andrés, M. T. Vijjapu, S. G. Surya, O. Shekhah, K. N. Salama, C. Serre, M. Eddaoudi, O. Roubeau and I. Gascón, Methanol and Humidity Capacitive Sensors Based on Thin Films of MOF Nanoparticles, *ACS Appl. Mater. Interfaces*, 2020, **12**(3), 4155–4162, DOI: 10.1021/ACSAMI.9B20763.

93 N. C. Burtch, J. Heinen, T. D. Bennett, D. Dubbeldam and M. D. Allendorf, Mechanical Properties in Metal–Organic Frameworks: Emerging Opportunities and Challenges for Device Functionality and Technological Applications, *Adv. Mater.*, 2018, **30**(37), 1704124, DOI: 10.1002/ADMA.201704124.

94 M. S. Denny, M. Kalaj, K. C. Bentz and S. M. Cohen, Multicomponent Metal–Organic Framework Membranes for Advanced Functional Composites, *Chem. Sci.*, 2018, **9**(47), 8842–8849, DOI: 10.1039/C8SC02356E.

95 J. R. Askim, M. Mahmoudi and K. S. Suslick, Optical Sensor Arrays for Chemical Sensing: The Optoelectronic Nose Chemical Society Reviews Optical Sensor Arrays for Chemical Sensing: The Optoelectronic Nose, *Chem. Soc. Rev.*, 2013, **42**, 8649, DOI: 10.1039/c3cs60179j.

96 Z. Wang and Q. Chen, Vapochromic Behavior of MOF for Selective Sensing of Ethanol, *Spectrochim. Acta, Part A*, 2018, **194**, 158–162, DOI: 10.1016/J.SAA.2017.12.072.

97 S. Tunsrichon, S. Youngme and J. Boonmak, Coexistence of Naked-Eye Mechanochromism, Vapochromism, and Thermochromism in a Soft Crystalline Layered Nickel(II) Coordination Polymer, *Inorg. Chem.*, 2021, **60**(23), 18242–18250, DOI: 10.1021/ACS.INORGCHEM.1C02875.

98 S. Nakatsuka, Y. Watanabe, Y. Kamakura, S. Horike, D. Tanaka and T. Hatakeyama, Solvent-Vapor-Induced Reversible Single-Crystal-to-Single-Crystal Transformation of a Triphosphaazatriangulene-Based Metal–Organic Framework, *Angew. Chem., Int. Ed.*, 2020, **59**(4), 1435–1439, DOI: 10.1002/ANIE.201912195.

99 Y. Yu, J. P. Ma, C. W. Zhao, J. Yang, X. M. Zhang, Q. K. Liu and Y. B. Dong, Copper(I) Metal-Organic Framework: Visual Sensor for Detecting Small Polar Aliphatic Volatile Organic Compounds, *Inorg. Chem.*, 2015, **54**(24), 11590–11592, DOI: 10.1021/ACS.INORGCHEM.5B02150.

100 N. N. Yang, W. Sun, F. G. Xi, Q. Sui, L. J. Chen and E. Q. Gao, Postsynthetic N-Methylation Making a Metal–Organic Framework Responsive to Alkylamines, *Chem. Commun.*, 2017, **53**(10), 1747–1750, DOI: 10.1039/C6CC10278F.

101 X. Y. Liu, X. M. Yin, S. L. Yang, L. Zhang, R. Bu and E. Q. Gao, Chromic and Fluorescence-Responsive Metal-Organic Frameworks Afforded by N-Amination Modification, *ACS Appl. Mater. Interfaces*, 2021, **13**(17), 20380–20387, DOI: 10.1021/ACSAMI.1C03937.

102 S. L. Li, M. Han, Y. Zhang, G. P. Li, M. Li, G. He and X. M. Zhang, X-Ray and UV Dual Photochromism, Thermochromism, Electrochromism, and Amine-Selective Chemochromism in an Anderson-Like Zn7 Cluster-Based 7-Fold Interpenetrated Framework, *J. Am. Chem. Soc.*, 2019, **141**(32), 12663–12672, DOI: 10.1021/JACS.9B04930.

103 C. Zhang, L. Sun, Y. Yan, Y. Liu, Z. Liang, Y. Liu and J. Li, Metal–Organic Frameworks Based on Bipyridinium Carboxylate: Photochromism and Selective Vapochromism, *J. Mater. Chem. C*, 2017, **5**(8), 2084–2089, DOI: 10.1039/C6TC04724F.

104 S. A. A. Razavi, M. Y. Masoomi and A. Morsali, Stimuli-Responsive Metal–Organic Framework (MOF) with Chemo-Switchable Properties for Colorimetric Detection of $CHCl_3$, *Chem.–Eur. J.*, 2017, **23**(51), 12559–12564, DOI: 10.1002/CHEM.201702127.

105 B. Gao, P. Hao, G. P. Li, J. Shen and Y. Fu, An Electron-Deficient Naphthalene Diimide-Based Metal–Organic Framework for Detecting Electron-Rich Molecules through Photo-/Chemo-Induced Chromism, *Dalton Trans.*, 2021, **50**(39), 13993–14000, DOI: 10.1039/D1DT02555D.

106 F. Moreau, J. Marrot, F. Banse, C. Serre and A. Tissot, Sequential Installation of Fe(II) Complexes in MOFs: Towards the Design of Solvatochromic Porous Solids, *J. Mater. Chem. C*, 2020, **8**(47), 16826–16833, DOI: 10.1039/D0TC03756G.

107 Z. Q. Yao, K. Wang, R. Liu, Y. J. Yuan, J. J. Pang, Q. W. Li, T. Y. Shao, Z. G. Li, R. Feng, B. Zou, W. Li, J. Xu and X. H. Bu, Dynamic Full-Color Tuning of Organic Chromophore in a Multi-Stimuli-Responsive 2D Flexible MOF, *Angew. Chem., Int. Ed.*, 2022, **61**(17), e202202073, DOI: 10.1002/ANIE.202202073.

108 C. Y. Liu, X. R. Chen, H. X. Chen, Z. Niu, H. Hirao, P. Braunstein and J. P. Lang, Ultrafast Luminescent Light-Up Guest Detection Based on the Lock of the Host Molecular Vibration, *J. Am. Chem. Soc.*, 2020, **142**(14), 6690–6697, DOI: 10.1021/JACS.0C00368.

109 J. F. Olorunyomi, M. M. Sadiq, M. Batten, K. Konstas, D. Chen, C. M. Doherty and R. A. Caruso, Advancing Metal-Organic Frameworks toward Smart Sensing: Enhanced Fluorescence by a Photonic Metal-Organic Framework for Organic Vapor Sensing, *Adv. Opt. Mater.*, 2020, **8**(19), 2000961, DOI: 10.1002/ADOM.202000961.

110 C. Li, L. Li, S. Yu, X. Jiao and D. Chen, High Performance Hollow Metal–Organic Framework Nanoshell-Based Etalons for Volatile Organic Compounds Detection, *Adv. Mater. Technol.*, 2016, **1**(7), 1600127, DOI: 10.1002/ADMT.201600127.

111 Z. Li, J. Liu, X. Yi, W. Wu, F. Li, Z. Zhu, H. Li, J. Shi, Y. Xu, F. Zhou and W. Liu, Metal–Organic Frameworks-Based Fabry–Pérot Cavity Encapsulated TiO_2 Nanoparticles for Selective Chemical Sensing, *Adv. Funct. Mater.*, 2022, **32**(9), 2109541, DOI: 10.1002/ADFM.202109541.

112 S. Yu, X. Wang, X. Jiao, C. Li and D. Chen, Polyhedral Metal–Organic Framework Monolayer Colloidal Crystals with Sharpened and Crystal Facet-Dependent Selectivity for Organic Vapor Sensing, *J. Mater. Chem. C*, 2021, **9**(16), 5379–5386, DOI: 10.1039/D1TC00810B.

113 A. Ranft, F. Niekiel, I. Pavlichenko, N. Stock and B. V. Lotsch, Tandem MOF-Based Photonic Crystals for

Open Access Article. Published on 05 lokakuuta 2022. Downloaded on 8.6.2026 20.57.17.
This article is licensed under a Creative Commons Attribution-NonCommercial 3.0 Unported Licence.

Enhanced Analyte-Specific Optical Detection, *Chem. Mater.*, 2015, **27**(6), 1961–1970, DOI: 10.1021/CM503640C.

114 A. Von Mankowski, K. Szendrei-Temesi, C. Koschnick and B. V. Lotsch, Improving Analyte Selectivity by Post-Assembly Modification of Metal–Organic Framework Based Photonic Crystal Sensors, *Nanoscale Horiz.*, 2018, **3**(4), 383–390, DOI: 10.1039/C7NH00209B.

115 O. Dalstein, D. R. Ceratti, C. Boissière, D. Grosso, A. Cattoni and M. Faustini, Nanoimprinted, Submicrometric, MOF-Based 2D Photonic Structures: Toward Easy Selective Vapors Sensing by a Smartphone Camera, *Adv. Funct. Mater.*, 2016, **26**(1), 81–90, DOI: 10.1002/ADFM.201503016.

116 O. Dalstein, E. Gkaniatsou, C. Sicard, O. Sel, H. Perrot, C. Serre, C. Boissière and M. Faustini, Evaporation-Directed Crack-Patterning of Metal-Organic Framework Colloidal Films and Their Application as Photonic Sensors Evaporation-Directed Crack-Patterning of Metal-Organic Framework Colloidal Films and Their Application as Photonic Sensors, *Angew. Chem., Int. Ed.*, 2017, **56**(45), DOI: 10.1002/anie.201706745ï.

117 X. Ma, J. Wu, L. Jiang, M. Wang, G. Deng, S. Qu and K. Chen, On-Chip Integration of a Metal–Organic Framework Nanomaterial on a SiO_2 Waveguide for Sensitive VOC Sensing, *Lab Chip*, 2021, **21**(17), 3298–3306, DOI: 10.1039/D1LC00503K.

118 Y. Huang, W. Lin, T. Huang, Z. Li, Z. Zhang, R. Xiao, X. Yang, S. Lian, J. Pan, J. Ma, W. Wang, L.-P. Sun, J. Li, B.-O. Guan, Y. Huang, W. F. Lin, T. S. Huang, Z. R. Li, Z. R. Zhang, R. T. Xiao, X. Yang, S. T. Lian, J. Ma, W. Wang, L.-P. Sun, J. Li, B.-O. Guan and J. S. Pan, Ultrafast Response Optical Microfiber Interferometric VOC Sensor Based on Evanescent Field Interaction with ZIF-8/Graphene Oxide Nanocoating, *Adv. Opt. Mater.*, 2022, **10**(3), 2101561, DOI: 10.1002/ADOM.202101561.

119 J. Wu, W. Zhang, Y. Wang, B. Li, T. Hao, Y. Zheng, L. Jiang, K. Chen and K. S. Chiang, Nanoscale Light–Matter Interactions in Metal–Organic Frameworks Cladding Optical Fibers, *Nanoscale*, 2020, **12**(18), 9991–10000, DOI: 10.1039/C9NR09061D.

120 W. Vandezande, K. P. F. Janssen, F. Delport, R. Ameloot, D. E. De Vos, J. Lammertyn and M. B. J. Roeffaers, Parts per Million Detection of Alcohol Vapors via Metal Organic Framework Functionalized Surface Plasmon Resonance Sensors, *Anal. Chem.*, 2017, **89**(8), 4480–4487, DOI: 10.1021/ACS.ANALCHEM.6B04510.

121 M. L. Tietze, M. Obst, G. Arnauts, N. Wauteraerts, S. Rodríguez-Hermida and R. Ameloot, Parts-per-Million Detection of Volatile Organic Compounds via Surface Plasmon Polaritons and Nanometer-Thick Metal–Organic Framework Films, *ACS Appl. Nano Mater.*, 2022, **5**(4), 5006–5016, DOI: 10.1021/ACSANM.2C00012.

122 C. Sher, L. Koh, H. K. Lee, X. Han, H. Yi, F. Sim, X. Y. Ling and R. Li, Plasmonic Nose: Integrating the MOF-Enabled Molecular Preconcentration Effect with a Plasmonic Array for Recognition of Molecular-Level Volatile Organic Compounds, *Chem. Commun.*, 2018, **54**(20), 2546–2549, DOI: 10.1039/C8CC00564H.

123 M. Lafuente, S. De Marchi, M. Urbiztondo, I. Pastoriza-Santos, I. Pérez-Juste, J. Santamaría, R. Mallada and M. Pina, Plasmonic MOF Thin Films with Raman Internal Standard for Fast and Ultrasensitive SERS Detection of Chemical Warfare Agents in Ambient Air, *ACS Sens.*, 2021, **6**(6), 2241–2251, DOI: 10.1021/ACSSENSORS.1C00178.

124 G. C. Phan-Quang, N. Yang, H. K. Lee, H. Y. F. Sim, C. S. L. Koh, Y. C. Kao, Z. C. Wong, E. K. M. Tan, Y. E. Miao, W. Fan, T. Liu, I. Y. Phang and X. Y. Ling, Tracking Airborne Molecules from Afar: Three-Dimensional Metal-Organic Framework-Surface-Enhanced Raman Scattering Platform for Stand-off and Real-Time Atmospheric Monitoring, *ACS Nano*, 2019, **13**(10), 12090–12099, DOI: 10.1021/ACSNANO.9B06486.

125 Q. Chen, Z. Chang, W. C. Song, H. Song, H. B. Song, T. L. Hu and X. H. Bu, A Controllable Gate Effect in Cobalt(II) Organic Frameworks by Reversible Structure Transformations, *Angew. Chem., Int. Ed.*, 2013, **52**(44), 11550–11553, DOI: 10.1002/ANIE.201306304.

126 C. N. Dzesse T, E. N. Nfor and S. A. Bourne, Vapor Sorption and Solvatochromism in a Metal-Organic Framework of an Asymmetric Pyridylcarboxylate, *Cryst. Growth Des.*, 2018, **18**(1), 416–423, DOI: 10.1021/ACS.CGD.7B01417.

127 B. Li, X. Chen, P. Hu, A. Kirchon, Y. M. Zhao, J. Pang, T. Zhang and H. C. Zhou, Facile Fabrication of a Multifunctional Metal-Organic Framework-Based Sensor Exhibiting Exclusive Solvochromic Behaviors toward Ketone Molecules, *ACS Appl. Mater. Interfaces*, 2019, **11**(8), 8227–8233, DOI: 10.1021/ACSAMI.8B19815.

128 Y. Shigeta, A. Kobayashi, T. Ohba, M. Yoshida, T. Matsumoto, H. C. Chang and M. Kato, Shape-Memory Platinum(II) Complexes: Intelligent Vapor-History Sensor with ON–OFF Switching Function, *Chem.–Eur. J.*, 2016, **22**(8), 2682–2690, DOI: 10.1002/CHEM.201503247.

129 Y. Shigeta, A. Kobayashi, M. Yoshida and M. Kato, Crystal Engineering of Vapochromic Porous Crystals Composed of Pt(II)-Diimine Luminophores for Vapor-History Sensors, *Cryst. Growth Des.*, 2018, **18**(6), 3419–3427, DOI: 10.1021/acs.cgd.8b00130.

130 G. X. Jin, J. Wang, J. Y. Liu, J. P. Ma and Y. B. Dong, Visual Recognition and Removal of C_2H_2 from C_2H_4/C_2H_2 Mixtures by a CuI-MOF, *Inorg. Chem.*, 2018, **57**(11), 6218–6221, DOI: 10.1021/ACS.INORGCHEM.8B00971.

131 P. Li, Q. Sui, M. Y. Guo, S. L. Yang, R. Bu and E. Q. Gao, Selective Chemochromic and Chemically-Induced Photochromic Response of a Metal–Organic Framework, *Chem. Commun.*, 2020, **56**(44), 5929–5932, DOI: 10.1039/D0CC01627F.

132 L. Li, Y. Hua, Y. Guo, H. Y. Wang, X. N. Li and H. Zhang, Bifunctional Photo- and Vapochromic Behaviors of a Novel Porous Zwitterionic Metal–Organic Framework, *New J. Chem.*, 2019, **43**(8), 3428–3431, DOI: 10.1039/C8NJ04905J.

133 M. Y. Guo, P. Li, S. L. Yang, R. Bu, X. Q. Piao and E. Q. Gao, Distinct and Selective Amine- and Anion-Responsive Behaviors of an Electron-Deficient and Anion-Exchangeable Metal–Organic Framework, *ACS Appl.*

© 2022 The Author(s). Published by the Royal Society of Chemistry

Open Access Article. Published on 05 lokakuuta 2022. Downloaded on 8.6.2026 20.57.17.
This article is licensed under a Creative Commons Attribution-NonCommercial 3.0 Unported Licence.

Mater. Interfaces, 2020, **12**(39), 43958–43966, DOI: **10.1021/ACSAMI.0C14648**.

134 Y. Feng, Y. Wang and Y. Ying, Structural Design of Metal–Organic Frameworks with Tunable Colorimetric Responses for Visual Sensing Applications, *Coord. Chem. Rev.*, 2021, **446**, 214102, DOI: **10.1016/J.CCR.2021.214102**.

135 X. D. Yang, R. Zhu, J. P. Yin, L. Sun, R. Y. Guo and J. Zhang, Bipyridinium-Bearing Multi-Stimuli Responsive Chromic Material with High Stability, *Cryst. Growth Des.*, 2018, **18**(5), 3236–3243, DOI: **10.1021/ACS.CGD.8B00390**.

136 S. Hu, J. Zhang, S. Chen, J. Dai and Z. Fu, *Efficient Ultraviolet Light Detector Based on a Crystalline Viologen-Based Metal–Organic Framework with Rapid Visible Color Change under Irradiation*, 2017, DOI: DOI: **10.1021/acsami.7b13367**.

137 Y. Zhang, M. Gutiérrezgutiérrez, A. K. Chaudhari and J.-C. Tan, Dye-Encapsulated Zeolitic Imidazolate Framework (ZIF-71) for Fluorochromic Sensing of Pressure, Temperature, and Volatile Solvents, *ACS Appl. Mater. Interfaces*, 2020, **12**, 37488, DOI: **10.1021/acsami.0c10257**.

138 X. Y. Liu, K. Xing, Y. Li, C. K. Tsung and J. Li, Three Models to Encapsulate Multicomponent Dyes into Nanocrystal Pores: A New Strategy for Generating High-Quality White Light, *J. Am. Chem. Soc.*, 2019, **141**(37), 14807–14813, DOI: **10.1021/JACS.9B07236**.

139 H. A. Schwartz, S. Olthof, D. Schaniel, K. Meerholz and U. Ruschewitz, Solution-Like Behavior of Photoswitchable Spiropyrans Embedded in Metal-Organic Frameworks, *Inorg. Chem.*, 2017, **56**(21), 13100–13110, DOI: **10.1021/ACS.INORGCHEM.7B01908**.

140 Y. Gao, M. Hilbers, H. Zhang and S. Tanase, Designed Synthesis of Multiluminescent Materials Using Lanthanide Metal-Organic Frameworks and Carbon Dots as Building-Blocks, *Eur. J. Inorg. Chem.*, 2019, **2019**(35), 3925–3932, DOI: **10.1002/EJIC.201900876**.

141 M. Gutiérrez, Y. Zhang and J.-C. Tan, Confinement of Luminescent Guests in Metal–Organic Frameworks: Understanding Pathways from Synthesis and Multimodal Characterization to Potential Applications of LG@MOF Systems, *Chem. Rev.*, 2022, **122**(11), 10438–10483, DOI: **10.1021/ACS.CHEMREV.1C00980**.

142 J. Su, S. Yuan, T. Wang, C. T. Lollar, J. L. Zuo, J. Zhang and H. C. Zhou, Zirconium Metal–Organic Frameworks Incorporating Tetrathiafulvalene Linkers: Robust and Redox-Active Matrices for In Situ Confinement of Metal Nanoparticles, *Chem. Sci.*, 2020, **11**(7), 1918–1925, DOI: **10.1039/C9SC06009J**.

143 M. C. De Koning, G. W. Peterson, M. Van Grol, I. Iordanov and M. McEntee, Degradation and Detection of the Nerve Agent VX by a Chromophore-Functionalized Zirconium MOF, *Chem. Mater.*, 2019, **31**(18), 7417–7424, DOI: **10.1021/ACS.CHEMMATER.9B02073**.

144 K. Ma, M. Van Grol, I. Iordanov, M. J. L. Kruijne, K. B. Idrees, H. Xie, T. Islamoglu, R. P. T. Bross and O. K. Farha, Development of a Metal-Organic Framework/Textile Composite for the Rapid Degradation and Sensitive Detection of the Nerve Agent VX, *Chem. Mater.*, 2022, **34**(3), 1269–1277, DOI: **10.1021/ACS.CHEMMATER.1C03895**.

145 Y. Gao, Y. Qi, K. Zhao, Q. Wen, J. Shen, L. Qiu and W. Mou, An Optical Sensing Platform for the Dual Channel Detection of Picric Acid: The Combination of Rhodamine and Metal-Organic Frameworks, *Sens. Actuators, B*, 2018, **257**, 553–560, DOI: **10.1016/J.SNB.2017.11.007**.

146 Y. Shu, Q. Ye, T. Dai, Q. Xu and X. Hu, Encapsulation of Luminescent Guests to Construct Luminescent Metal-Organic Frameworks for Chemical Sensing, *ACS Sens.*, 2021, **6**(3), 641–658, DOI: **10.1021/ACSSENSORS.0C02562**.

147 T. Zhao, I. Boldog, V. Spasojevic, A. Rotaru, Y. Garcia and C. Janiak, Solvent-Triggered Relaxative Spin State Switching of $[Fe(HB(Pz)_3)_2]$ in a Closed Nano-Confinement of NH_2-MIL-101(Al), *J. Mater. Chem. C*, 2016, **4**(27), 6588–6601, DOI: **10.1039/c6tc01297c**.

148 A. Tissot, X. Kesse, S. Giannopoulou, I. Stenger, L. Binet, E. Rivière and C. Serre, A Spin Crossover Porous Hybrid Architecture for Potential Sensing Applications, *Chem. Commun*, 2019, **55**, 194–197, DOI: **10.1039/c8cc07573e**.

149 Y. Cui, J. Zhang, H. He and G. Qian, Photonic Functional Metal-Organic Frameworks, *Chem. Soc. Rev.*, 2018, 5740–5785, DOI: **10.1039/c7cs00879a**.

150 J.-X. Wang, J. Yin, O. Shekhah, O. M. Bakr, M. Eddaoudi and O. F. Mohammed, Energy Transfer in Metal–Organic Frameworks for Fluorescence Sensing, *ACS Appl. Mater. Interfaces*, 2022, **14**(8), 9970–9986, DOI: **10.1021/ACSAMI.1C24759**.

151 W. P. Lustig, S. Mukherjee, N. D. Rudd, A. V. Desai, J. Li and S. K. Ghosh, Metal–Organic Frameworks: Functional Luminescent and Photonic Materials for Sensing Applications, *Chem. Soc. Rev.*, 2017, **46**(11), 3242–3285, DOI: **10.1039/C6CS00930A**.

152 G. L. Yang, X. L. Jiang, H. Xu and B. Zhao, Applications of MOFs as Luminescent Sensors for Environmental Pollutants, *Small*, 2021, **17**(22), 1–19, DOI: **10.1002/smll.202005327**.

153 B. Yan, Luminescence Response Mode and Chemical Sensing Mechanism for Lanthanide-Functionalized Metal–Organic Framework Hybrids, *Inorg. Chem. Front.*, 2021, **8**(1), 201–233, DOI: **10.1039/D0QI01153C**.

154 G. A. Leith, C. R. Martin, J. M. Mayers, P. Kittikhunnatham, R. W. Larsen and N. B. Shustova, Confinement-Guided Photophysics in MOFs, COFs, and Cages, *Chem. Soc. Rev.*, 2021, **50**(7), 4382–4410, DOI: **10.1039/D0CS01519A**.

155 R. Haldar, L. Heinke, C. Wöll, R. Haldar, L. Heinke and C. Wöll, Advanced Photoresponsive Materials Using the Metal–Organic Framework Approach, *Adv. Mater.*, 2020, **32**(20), 1905227, DOI: **10.1002/ADMA.201905227**.

156 R.-B. Lin, S.-Y. Liu, J.-W. Ye, X.-Y. Li, J.-P. Zhang, R.-B. Lin, S.-Y. Liu, J.-W. Ye, X.-Y. Li and J.-P. Zhang, Photoluminescent Metal–Organic Frameworks for Gas Sensing, *Adv. Sci.*, 2016, **3**(7), 1500434, DOI: **10.1002/ADVS.201500434**.

157 S. Khatua, C. Krishnaraj, D. C. Baruah, P. Van Der Voort and H. S. Jena, Flexible Luminescent Non-Lanthanide Metal–Organic Frameworks as Small Molecules Sensors,

Open Access Article. Published on 05 lokakuuta 2022. Downloaded on 8.6.2026 20.57.17.
This article is licensed under a Creative Commons Attribution-NonCommercial 3.0 Unported Licence.

Dalton Trans., 2021, **50**(41), 14513–14531, DOI: 10.1039/D1DT03175A.

158 H. Wang, W. P. Lustig and J. Li, Sensing and Capture of Toxic and Hazardous Gases and Vapors by Metal–Organic Frameworks, *Chem. Soc. Rev.*, 2018, **47**(13), 4729–4756, DOI: 10.1039/C7CS00885F.

159 T. Rasheed and F. Nabeel, Luminescent Metal-Organic Frameworks as Potential Sensory Materials for Various Environmental Toxic Agents, *Coord. Chem. Rev.*, 2019, **401**, 213065, DOI: 10.1016/j.ccr.2019.213065.

160 Y. Zhang, S. Yuan, G. Day, X. Wang, X. Yang, H.-C. Zhou and H.-C. Zhou, Luminescent Sensors Based on Metal-Organic Frameworks, *Coord. Chem. Rev.*, 2018, **354**, 28–45, DOI: 10.1016/j.ccr.2017.06.007.

161 B. H. Bunch and A. Hellemans, *The History of Science and Technology*, Houghton Mifflin Company, 2004.

162 C. Zhu, R. E. Gerald and J. Huang, Metal-Organic Framework Materials Coupled to Optical Fibers for Chemical Sensing: A Review, *IEEE Sens. J.*, 2021, **21**(18), 19647–19661, DOI: 10.1109/JSEN.2021.3094092.

163 G. Lu and J. T. Hupp, Metal-Organic Frameworks as Sensors: A ZIF-8 Based Fabry-Pérot Device as a Selective Sensor for Chemical Vapors and Gases, *J. Am. Chem. Soc.*, 2010, **132**(23), 7832–7833, DOI: 10.1021/JA101415B.

164 R. Zhang, D. Zhang, Y. Yao, Q. Zhang, Y. Xu, Y. Wu, H. Yu and G. Lu, Metal–Organic Framework Crystal-Assembled Optical Sensors for Chemical Vapors: Effects of Crystal Sizes and Missing-Linker Defects on Sensing Performances, *ACS Appl. Mater. Interfaces*, 2019, **11**, 28, DOI: 10.1021/acsami.9b05933.

165 G. Lu, O. K. Farha, L. E. Kreno, P. M. Schoenecker, K. S. Walton, R. P. Van Duyne and J. T. Hupp, Fabrication of Metal-Organic Framework-Containing Silica-Colloidal Crystals for Vapor Sensing, *Adv. Mater.*, 2011, **23**(38), 4449–4452, DOI: 10.1002/ADMA.201102116.

166 L. Li, X. Jiao, D. Chen, B. V. Lotsch and C. Li, Facile Fabrication of Ultrathin Metal-Organic Framework-Coated Monolayer Colloidal Crystals for Highly Efficient Vapor Sensing, *Chem. Mater.*, 2015, **27**(22), 7601–7609, DOI: 10.1021/ACS.CHEMMATER.5B02476.

167 Z. Wang, J. Zhang, J. Xie, C. Li, Y. Li, S. Liang, Z. Tian, T. Wang, H. Zhang, H. Li, W. Xu and B. Yang, Bioinspired Water-Vapor-Responsive Organic/Inorganic Hybrid One-Dimensional Photonic Crystals with Tunable Full-Color Stop Band, *Adv. Funct. Mater.*, 2010, **20**(21), 3784–3790, DOI: 10.1002/ADFM.201001195.

168 D. Kou, W. Ma, S. Zhang, R. Li and Y. Zhang, BTEX Vapor Detection with a Flexible MOF and Functional Polymer by Means of a Composite Photonic Crystal, *ACS Appl. Mater. Interfaces*, 2020, **12**(10), 11955–11964, DOI: 10.1021/ACSAMI.9B22033.

169 F. M. Hinterholzinger, A. Ranft, J. M. Feckl, B. Rühle, T. Bein and B. V. Lotsch, One-Dimensional Metal–Organic Framework Photonic Crystals Used as Platforms for Vapor Sorption, *J. Mater. Chem.*, 2012, **22**(20), 10356–10362, DOI: 10.1039/C2JM15685G.

170 Z. Hu, C. A. Tao, F. Wang, X. Zou and J. Wang, Flexible Metal–Organic Framework-Based One-Dimensional Photonic Crystals, *J. Mater. Chem. C*, 2014, **3**(1), 211–216, DOI: 10.1039/C4TC01501K.

171 G. Lu, O. K. Farha, W. Zhang, F. Huo and J. T. Hupp, Engineering ZIF-8 Thin Films for Hybrid MOF-Based Devices, *Adv. Mater.*, 2012, **24**(29), 3970–3974, DOI: 10.1002/ADMA.201202116.

172 Y.-N. Wu, F. Li, W. Zhu, J. Cui, C.-A. Tao, C. Lin, P. M. Hannam, G. Li, Y. Wu, F. Li, P. M. Hannam, Y. Wu, W. Zhu, J. Cui, C. Tao, C. Lin and G. Li, Metal–Organic Frameworks with a Three-Dimensional Ordered Macroporous Structure: Dynamic Photonic Materials, *Angew. Chem., Int. Ed.*, 2011, **50**(52), 12518–12522, DOI: 10.1002/ANIE.201104597.

173 Z. Wang, K. Zhan, Y. Zhu, J. Yan, B. Liu and Y. Chen, Label-Free One-Dimension Photonics Crystals Sensors Assembled by UiO-66 and Graphene Oxide: A Platform to Quick and Efficiently Detect Chlorobenzene Vapors, *J. Environ. Chem. Eng.*, 2021, **9**(4), 105445, DOI: 10.1016/J.JECE.2021.105445.

174 Y. Xing, Z. Wang, Y. Zhu, J. Yan and Y. Chen, High-Performance Chlorobenzene Sensor of Bimetallic ZIF-8(Zn@Co) Based One-Dimensional Photonic Crystals, *Phys. Lett. A*, 2021, **400**, 127301, DOI: 10.1016/J.PHYSLETA.2021.127301.

175 L. Bai, Y. He, J. Zhou, Y. Lim, V. C. Mai, Y. Chen, S. Hou, Y. Zhao, J. Zhang and H. Duan, Responsive Amorphous Photonic Structures of Spherical/Polyhedral Colloidal Metal–Organic Frameworks, *Adv. Opt. Mater.*, 2019, **7**(13), 1–8, DOI: 10.1002/adom.201900522.

176 K. J. Kim, P. Lu, J. T. Culp and P. R. Ohodnicki, Metal-Organic Framework Thin Film Coated Optical Fiber Sensors: A Novel Waveguide-Based Chemical Sensing Platform, *ACS Sens.*, 2018, **3**(2), 386–394, DOI: 10.1021/ACSSENSORS.7B00808.

177 O. Guselnikova, S. Chufistova, Z. Kolska, R. Elashnikov, V. Burtsev, P. Postnikov, V. Svorcik and O. Lyutakov, Fast and All-Optical Hydrogen Sensor Based on Gold-Coated Optical Fiber Functionalized with Metal-Organic Framework Layer, *ACS Sens.*, 2019, **4**(12), 3133–3140, DOI: 10.1021/ACSSENSORS.9B01074.

178 K. J. Kim, J. T. Culp, P. R. Ohodnicki, P. C. Cvetic, S. Sanguinito, A. L. Goodman and H. T. Kwon, Alkylamine-Integrated Metal-Organic Framework-Based Waveguide Sensors for Efficient Detection of Carbon Dioxide from Humid Gas Streams, *ACS Appl. Mater. Interfaces*, 2019, **11**(36), 33489–33496, DOI: 10.1021/ACSAMI.9B12052.

179 H.-T. Kim, W. Hwang, Y. Liu and A. M. Yu, Ultracompact Gas Sensor with Metal-Organic-Framework-Based Differential Fiber-Optic Fabry-Perot Nanocavities, *Opt. Express*, 2020, **28**(20), 29937–29947, DOI: 10.1364/OE.396146.

180 C. Zhu, J. A. Perman, R. E. Gerald, S. Ma and J. Huang, Chemical Detection Using a Metal-Organic Framework Single Crystal Coupled to an Optical Fiber, *ACS Appl.*

© 2022 The Author(s). Published by the Royal Society of Chemistry

Open Access Article. Published on 05 lokakuuta 2022. Downloaded on 8.6.2026 20.57.17.
This article is licensed under a Creative Commons Attribution-NonCommercial 3.0 Unported Licence.

Mater. Interfaces, 2019, **11**(4), 4393–4398, DOI: 10.1021/ACSAMI.8B19775.

181 R. Cao, H. Ding, K. J. Kim, Z. Peng, J. Wu, J. T. Culp, P. R. Ohodnicki, E. Beckman and K. P. Chen, Metal-Organic Framework Functionalized Polymer Coating for Fiber Optical Methane Sensors, *Sens. Actuators, B*, 2020, **324**, 128627, DOI: 10.1016/J.SNB.2020.128627.

182 T. Martan, J. Aubrecht, O. Podrazký, V. Matějec and I. Kašík, Detection of Hydrocarbons Using Suspended Core Microstructured Optical Fiber, *Sens. Actuators, B*, 2014, **202**, 123–128, DOI: 10.1016/J.SNB.2014.04.103.

183 J. Wu, C. Tang, W. Zhang, X. Ma, S. Qu, K. Chen, T. Hao and K. S. Chiang, Lab on Optical Fiber: Surface Nano-Functionalization for Real-Time Monitoring of VOC Adsorption/Desorption in Metal-Organic Frameworks, *Nanophotonics*, 2021, **10**(10), 2705–2716, DOI: 10.1515/NANOPH-2021-0192.

184 J. Hromadka, B. Tokay, S. James, R. P. Tatam and S. Korposh, Optical Fibre Long Period Grating Gas Sensor Modified with Metal Organic Framework Thin Films, *Sens. Actuators, B*, 2015, **221**, 891–899, DOI: 10.1016/J.SNB.2015.07.027.

185 J. Hromadka, B. Tokay, R. Correia, S. P. Morgan and S. Korposh, Highly Sensitive Volatile Organic Compounds Vapour Measurements Using a Long Period Grating Optical Fibre Sensor Coated with Metal Organic Framework ZIF-8, *Sens. Actuators, B*, 2018, **260**, 685–692, DOI: 10.1016/J.SNB.2018.01.015.

186 L. E. Kreno, J. T. Hupp and R. P. Van Duyne, Metal-Organic Framework Thin Film for Enhanced Localized Surface Plasmon Resonance Gas Sensing, *Anal. Chem.*, 2010, **82**(19), 8042–8046, DOI: 10.1021/AC102127P.

187 C. S. L. Koh, H. Y. F. Sim, S. X. Leong, S. K. Boong, C. Chong and X. Y. Ling, Plasmonic Nanoparticle-Metal-Organic Framework (NP-MOF) Nanohybrid Platforms for Emerging Plasmonic Applications, *ACS Mater. Lett.*, 2021, **3**(5), 557–573, DOI: 10.1021/acsmaterialslett.1c00047.

188 C. Huang, A. Li, X. Chen, T. Wang, C. H. Huang, A. L. Li, X. Y. Chen and T. Wang, Understanding the Role of Metal–Organic Frameworks in Surface-Enhanced Raman Scattering Application, *Small*, 2020, **16**(43), 2004802, DOI: 10.1002/SMLL.202004802.

189 H. Lai, G. Li, F. Xu and Z. Zhang, Metal–Organic Frameworks: Opportunities and Challenges for Surface-Enhanced Raman Scattering – A Review, *J. Mater. Chem. C*, 2020, **8**(9), 2952–2963, DOI: 10.1039/D0TC00040J.

190 J. Langer, D. J. de Aberasturi, J. Aizpurua, R. A. Alvarez-Puebla, B. Auguié, J. J. Baumberg, G. C. Bazan, S. E. J. Bell, A. Boisen, A. G. Brolo, J. Choo, D. Cialla-May, V. Deckert, L. Fabris, K. Faulds, F. Javier García de Abajo, R. Goodacre, D. Graham, A. J. Haes, C. L. Haynes, C. Huck, T. Itoh, M. Käll, J. Kneipp, N. A. Kotov, H. Kuang, E. C. Le Ru, H. K. Lee, J. F. Li, X. Y. Ling, S. A. Maier, T. Mayerhöfer, M. Moskovits, K. Murakoshi, J. M. Nam, S. Nie, Y. Ozaki, I. Pastoriza-Santos, J. Perez-Juste, J. Popp, A. Pucci, S. Reich, B. Ren, G. C. Schatz, T. Shegai, S. Schlücker, L. L. Tay, K. George Thomas, Z. Q. Tian, R. P. van Duyne, T. Vo-Dinh, Y. Wang, K. A. Willets, C. Xu, H. Xu, Y. Xu, Y. S. Yamamoto, B. Zhao and L. M. Liz-Marzán, Present and Future of Surface-Enhanced Raman Scattering, *ACS Nano*, 2020, **14**(1), 28–117, DOI: 10.1021/ACSNANO.9B04224.

191 J. W. M. Osterrieth, D. Wright, H. Noh, C. W. Kung, D. Vulpe, A. Li, J. E. Park, R. P. Van Duyne, P. Z. Moghadam, J. J. Baumberg, O. K. Farha and D. Fairen-Jimenez, Core-Shell Gold Nanorod@Zirconium-Based Metal-Organic Framework Composites as In Situ Size-Selective Raman Probes, *J. Am. Chem. Soc.*, 2019, **141**(9), 3893–3900, DOI: 10.1021/JACS.8B11300.

192 D. Li, X. Cao, Q. Zhang, X. Ren, L. Jiang, D. Li, W. Deng and H. Liu, Facile In Situ Synthesis of Core–Shell MOF@Ag Nanoparticle Composites on Screen-Printed Electrodes for Ultrasensitive SERS Detection of Polycyclic Aromatic Hydrocarbons, *J. Mater. Chem. A*, 2019, **7**(23), 14108–14117, DOI: 10.1039/C9TA03690C.

193 Q. Q. Chen, R. N. Hou, Y. Z. Zhu, X. T. Wang, H. Zhang, Y. J. Zhang, L. Zhang, Z. Q. Tian and J. F. Li, Au@ZIF-8 Core-Shell Nanoparticles as a SERS Substrate for Volatile Organic Compound Gas Detection, *Anal. Chem.*, 2021, **93**(19), 7188–7195, DOI: 10.1021/ACS.ANALCHEM.0C05432.

194 X. Yang, Y. Liu, S. H. Lam, J. Wang, S. Wen, C. Yam, L. Shao and J. Wang, Site-Selective Deposition of Metal-Organic Frameworks on Gold Nanobipyramids for Surface-Enhanced Raman Scattering, *Nano Lett.*, 2021, **21**(19), 8205–8212, DOI: 10.1021/ACS.NANOLETT.1C02649.

195 H. Zhou, X. Hui, D. Li, D. Hu, X. Chen, X. He, L. Gao, H. Huang, C. Lee and X. Mu, Metal–Organic Framework-Surface-Enhanced Infrared Absorption Platform Enables Simultaneous On-Chip Sensing of Greenhouse Gases, *Adv. Sci.*, 2020, **7**(20), 2001173, DOI: 10.1002/ADVS.202001173.

© 2022 The Author(s). Published by the Royal Society of Chemistry